Photodiagnosis and Photodynamic Therapy 28 (2019) 38–52

Contents lists available at ScienceDirect

Photodiagnosis and Photodynamic Therapy

journal homepage: www.elsevier.com/locate/pdpdt

Importance of Hypericin-Bcl2 interactions for biological effects at subcellular levels

Katarina Stroffekova[a,*], Silvia Tomkova[a], Veronika Huntosova[b], Tibor Kozar[b]

[a] Department of Biophysics, Faculty of Natural Sciences, PJ Safarik University, Jesenna 5, Kosice, Slovakia
[b] Center of Interdisciplinary Biosciences, TIP-Safarik University, Jesenna 5, Kosice, Slovakia

ARTICLE INFO

Keywords:
Apoptosis
Hypericin light-independent effects
Bcl2 protein-ligand interaction
BH3 mimetics
Molecular modeling

ABSTRACT

Hypericin (Hyp) is a naturally occurring compound used as photosensitizer in photodynamic therapy and diagnosis. Recently, we have shown that Hyp presence alone, without illumination, resulted in substantial biological effects at several sub-cellular levels. Hyp induced changes in cellular ultrastructure, mitochondria function and metabolism, and distribution of Bcl2 proteins in malignant and non-malignant cells. The molecular mechanisms that underlie Hyp light-independent effects are still elusive. We have hypothesized that Bcl2-Hyp interactions might be one possible mechanism.

We performed molecular docking studies to determine the Hyp-Bcl2 interaction profile. Based on the interaction profiles small Bcl2 peptide segments were selected for further study. We designed small peptides corresponding to Bcl2 BH3 and BH1 domains and tested the binding of Hyp and Bcl2 known inhibitor, ABT263, to the peptides in computer modeling and *in vitro* binding studies. We employed endogenous tryptophan and tyrosine in the BH3 and BH1 peptides, respectively, and their fluorescent properties to show interaction with Hyp and ABT263.

Overall, our results indicate that Hyp can interact with Bcl2 protein at its BH3-BH1 hydrophobic groove, and this interaction may trigger changes in intracellular distribution of Bcl2 proteins. In addition, our computer modeling results suggest that Hyp also interacts with other anti-apoptotic members of Bcl2 family similar to the known BH3 mimetics. Our findings are novel and might contribute to understanding Hyp light-independent effects. In addition, they may substantiate the therapeutic use of Hyp as a BH3 mimetic molecule to enhance other cancer treatments.

1. Introduction

Members of the Bcl2 family of proteins are key regulators of apoptosis acting either as promoters or as suppressors of cell death. They are globular proteins containing α-helixes and one to four Bcl2 homology (BH) domains [1]. The specific BH domain presence and the ability to promote or suppress apoptosis have been used to sort the Bcl2 family members into three subgroups: anti-apoptotic, pro-apoptotic, and BH3-only proteins. Anti-apoptotic (Bcl2, Bcl_{XL}, Bclw, Mcl-1, A1, Bcl-B) and pro-apoptotic (Bax, Bak and possibly Bok) proteins are multi BH domains proteins. They contain highly conserved BH1, BH2 domains, and the least conserved BH4 domain. The BH3 motif defines pro-apoptotic activity and is present in all pro-apoptotic proteins and in some pro-survival ones. The BH3-only proteins have been shown to fulfill role of either sensitizer (Bad, Bmf, Puma, Noxa, Bik, Hrk) or direct activator (Bim, tBid) of pro-apoptotic Bax and Bak [2,3].

Cancer cells evade apoptosis by upregulating expression and activity of anti-apoptotic Bcl2 proteins (Bcl2, Bcl_{XL} and Mcl1) [4–6], and at the same time, this upregulation also results in simultaneous high-level expression of pro-apoptotic members of the family that “prime” cells for death [3]. Bcl2 homology domains are also present in several cancer-associated viruses that include Epstein–Barr and Kaposi sarcoma, suggesting that anti-apoptotic Bcl2 proteins may also participate in virus-induced cancer [7–9].

The intricate network of protein-protein interactions between multi BH domain anti- and pro-apoptotic Bcl2 proteins, and/or BH3-only proteins control cell survival or death via regulation of mitochondria function and fission/fusion processes [3]. The cell susceptibility to submit apoptosis strongly depends on the BH3-only proteins presence and their interaction with anti-apoptotic members. Cells, which have their anti-apoptotic Bcl2 proteins engaged with BH3-only activators, are termed as “primed for death”, and are likely to undergo apoptosis

* Corresponding Author.
E-mail address: katarina.stroffekova@upjs.sk (K. Stroffekova).

https://doi.org/10.1016/j.pdpdt.2019.08.016
Received 15 May 2019; Received in revised form 18 July 2019; Accepted 12 August 2019
Available online 17 August 2019

[2]. Several models were described to explain the protein interactions between members of Bcl2 family and how they regulate the mitochondria integrity and dynamics [2,3,10,11].

The BH3 motifs of pro-apoptotic proteins bind to the hydrophobic groove of their pro-survival partners, which is comprised of BH1, BH2 and BH3 domains [1]. The strength of interaction between the anti-apoptotic protein and BH3 motif can be either highly selective or quite promiscuous. Some BH3 motifs show promiscuous binding to all pro-survival Bcl2 proteins, whereas others are highly selective [12]. The importance of interaction between pro-survival Bcl2 proteins and BH3 motifs of either pro-apoptotic or BH3 only proteins for cell death or survival decisions makes this interaction an appealing target for cancer therapy. Multiple approaches have been used to alter pro-survival Bcl2 proteins and various BH3 motifs interactions. Peptides mimicking BH3 motifs of pro-apoptotic Bak, Bax or BH3-only proteins [9,13,14], or small molecule inhibitors of pro-survival Bcl2 proteins, termed as BH3 mimetics, were explored [15–19]. The BH3 mimetics described so far were designed as inhibitors of anti-apoptotic Bcl2 proteins (Bcl2, Bcl_{XL} and Mcl1), and thus function as apoptosis inducers/BH3 sensitizers [20]. More than 20 small molecules targeting Bcl2 family members are currently used in preclinical and clinical studies [19,21]. There are numbers of BH3 mimetics with diverse chemical structures available [20], which are either artificially synthetized (HA14-1, ABT 737 and 263, BI-21C6) [15,22–25], or naturally occurring (Gossypol, Chelerythrine, Antimycin A) [18,26–29]. Molecular structures of selected BH3 mimetics together with their predicted conformational flexibility are shown in Fig. 1. It is very likely that the number of BH3 mimetics will grow. In the present work, we present, for the first time, evidence that Hypericin (Hyp) (Hyp structure in Fig. 1) may be considered a promising naturally occurring BH3 mimetic.

Hypericin (Hyp) is a photosensitive phenanthroperylenquinone, naturally occurring in plants of the genus *Hypericum perforatum*. Hyp is used as a photosensitizer in photodynamic therapy (PDT) of tumors, inflammatory diseases, and infections [30,31]. Originally, Hyp and its derivates were considered compounds with a minimal cytotoxicity prior illumination. However, there is growing evidence to contrary, including our recent work [32–37]. Hypericin, due to its hydrophobic properties, crosses the cell membrane and accumulates mainly in membranous organelles such as ER, mitochondria, Golgi apparatus and lysosomes, where members of Bcl2 family have been shown to be present [38–42]. Recently, we have shown that Hyp presence alone in the malignant and nonmalignant cells resulted in significant effects on ultrastructure, mitochondria function and metabolism, and Bcl2 proteins´ distribution and synthesis (Huntosova, Novotova et al. 2017). In addition, Hyp was shown to have cytotoxic effects at concentrations from 0.5 μg/ml to 20 μg/ml, to decrease Bcl2 expression and to increase expression of metalloproteases ADAMTS1 and ADAMTS3 in breast cancer MCF7 cells [43,44]. The increased ADAMTS1 and ADAMTS3 expression was suggested to prevent metastasis and facilitate tumor suppression [44]. Further, Hyp displayed significantly higher accumulation in primary and metastatic tumors of lungs and bladder in comparison with normal tissues in *in vivo* and *in vitro* studies. Hyp also exhibited potent anti-proliferative and anti-metastatic effects without light activation [45–47]. In studies with neuronal tissue, Hyp preferentially accumulated in glial and connective tissues including glioma tumors, and poorly penetrated into neurons [48,49].

There are multiple molecular mechanisms underlying Hyp light-independent effects, including interaction between Hyp and proteins, which are not well understood. We have hypothesized that Bcl2-Hyp interactions might be one possible mechanism.

Despite decades of research regarding Hyp effects in the cells [30,31,50], there are not that many proteins known to directly interact with Hyp. In cells, Hyp displayed high reactivity towards two families of distantly related protein kinases: receptor-tyrosine kinases (EGF-R and Ins-R) and Ser/Thr protein kinases (PKC and MAP kinase); and to glutathione S-transferase (GST) [51–53]. It was shown that Hyp interacts with proteins from body fluids such as human serum albumin (HSA), hemoglobin, LDL apoB-100 protein, and with protein in eye lens α-crystallin [54–58]. Recently, others and we have shown that Hyp also interacts with P-glycoprotein and influences its activity [59,60]. Hyp binding sites in the afore mentioned proteins engage hydrophobic and hydrogen bond interactions between Hyp and protein binding domains [54,58,60,61].

Here, we investigated a possibility that Hyp interacts with the anti-apoptotic Bcl2 via its hydrophobic groove similar to BH3 mimetic ABT263. Our findings indicate that this interaction shows dominance of the hydrophobic interactions.

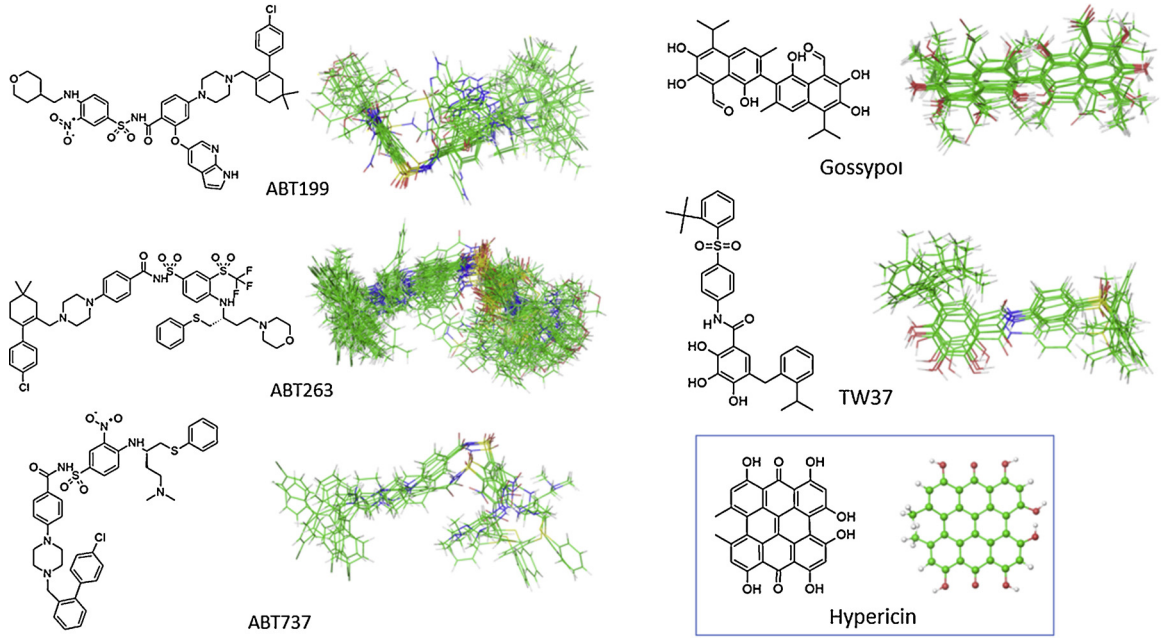

Fig. 1. 2D chemical structure comparison of selected BH3 mimetics and hypericin. Chemical structures are in **black** and their conformational sampling in **color** schemes.

2. Materials and methods

2.1. Cell culture and reagents

Primary culture of normal human coronary artery endothelial cells (*HCAEC*, Clonetics™) and endothelial growth medium (EGM™) supplemented with growth supplements (2-MV BulletKit™) were purchased from LONZA (France). An immortal cell line culture of malignant *U87 MG* human glioma cells was purchased from Cell Lines Services (CLS, Germany). Dulbecco´s modified Eagle medium (D-MEM) with high glucose (4500 mg.L^{-1}) was obtained from Life Technologies LTD (Slovakia) and FBS was purchased from Sigma Aldrich (Slovakia). Hyp was purchased from Gibco-Invitrogen (France), ABT263 (Navitoclax) was purchased from Selleckchem (Austria). Specific antibody against Bcl2 (anti-Bcl2-100, Sigma-Aldrich, Slovakia) and 3-(4,5-Dimethyl-2-thiazolyl)-2,5-diphenyl-2H-tetrazolium bromide (MTT reagent) were obtained from Sigma Aldrich (Slovakia). Secondary anti-mouse Ab conjugated with either Alexa Fluor 488 or Alexa Fluor 546 were obtained from Life Technologies, LTD (Slovakia).

Cells were plated and maintained according to propagation protocols onto 35 mm culture dishes with integral No.0 glass cover slip bottoms (MatTek, USA). The cells grew in the dark as monolayer up to 80% confluence, at 37 °C in a humidified 5% CO_2 atmosphere. After reaching confluence, cells were incubated with either Hyp or ABT263 and then processed either in the MTT assay, or by immunocytochemistry protocol.

2.2. Hypericin and ABT263 protocol

Hyp and ABT263 stock solutions were in dimethyl sulfoxide (DMSO) at concentration of 1×10^{-3} and 1×10^{-2}M, respectively. Hyp and ABT263 were further diluted to final concentrations of 0.5, 1 and 10 μM in the appropriate cell culture medium. For all experiments, the final content of DMSO was less than 0.1%. Cells were incubated with either Hyp or ABT263 for 1, 6 or 24 h in the dark in the presence of 5% CO_2 humidified atmosphere at 37 °C.

2.3. Immunocytochemistry protocol

Cells were fixed with 100% methanol at −20 °C for a minimum of 20 min. Cells were then stained by standard protocols [40] with specific primary antibody against Bcl2 (anti-Bcl2-100) and with appropriate secondary Abs conjugated with either Alexa 488 or Alexa 555.

2.4. MTT cell viability assay

HCAEC and U87 MG cells (2×10^3 cells per well) were plated in 96-well plates. Appropriate culture medium with or without either Hyp or ABT263 was added to the each well, and cells were incubated at 37 °C for the indicated times. After incubation with Hyp or ABT263 cell viability was determined via MTT assay. MTT stock solution was at concentration 5 mg/ml in PBS. After incubation with Hyp or ABT263, media from wells was removed, MTT was first diluted in fresh serum free medium (1:10) and then added into each well to a final volume of 100 μl. Cells were then incubated for 2 h in the dark in the presence of 5% CO_2 humidified atmosphere at 37 °C. Yellowish solution of MTT is converted to dark blue, water-insoluble crystals of MTT formazan by mitochondrial dehydrogenases in live cells. To dissolve the crystals, we added acidified isopropanol to each well. The absorbance of soluble formazan was measured at 590 nm with a microplate reader (GloMax, Promega). Cell viability is presented as the percentage of treated cells relative to the control ones.

2.5. Confocal microscopy

Cells were assessed with a 63X oil objective (NA = 1.46) of LSM 700 confocal microscope system (LSM 700, Zeiss Germany). The solid-state laser line (488 nm), and argon laser line (555 nm) were used to excite Alexa 488 and Alexa 555 fluorophores, respectively. Alexa 488 and Alexa 555 emissions were recorded in single-track configuration with a band-pass filter of 490–555 nm, or a long-pass filter of 575 nm, respectively. Fluorescence signals were analyzed by Zen 2011 software (Zeiss, Germany).

2.6. Molecular modeling

The 2013 Schrodinger Suite of programs [62] was used to determine the Bcl2/ligand interaction profile. The PDB 4IEH structure [63] for Bcl2 was processed using the “Protein Preparation” option of Maestro. The structures of Bcl_{XL} and Mcl1 were processed in similar way. The possible proteins binding sites were then determined using the SiteMap [64,65] program of Schrodinger suite [62]. Conformational analysis of the ligands was carried out by “MacroModel/Conformational Search” option of Maestro [62]. The preferred conformation geometry was then *ab initio* (DFT 6-31G** B3LYP) optimized with Jaguar [66] program. The obtained structures were first docked into the protein binding sites using program Glide, followed by QPLD (**Q**uantum **P**olarized **L**igand **D**ocking) protocol, which is based on combined QC/MM methodology [67].

Based on the protein-ligand interaction profiles small peptide segments of Bcl2 were selected for further study. Their geometries were used in two ways: a) in conserved geometry as seen in the original 4IEH PDB structure, and b) *de novo* predicted conformations of the corresponding sequences (Fig. 4A) using the protein fold modeling web page http://bioserv.rpbs.univ-paris-diderot.fr/services/PEP-FOLD3/. This modeling resulted in a few hundred conformations of the wild type and scrambled peptides, creating four groups of small peptide conformations entitled wBH1, scBH1, wBH3, scBH3.

Hypericin and ABT263 were then docked into all binding sites of all wBH1, scBH1, wBH3, scBH3 peptide conformations using the Autodock VINA tool [68]. The PLIP [69] program was then used to analyze the protein-ligand interaction profiles of hundreds peptide-ligand complexes resulted from Autodock VINA runs.

The Autodock VINA preferred pose geometries of Hypericin and ABT263 and wBH1, scBH1, wBH3, scBH3 peptides, were used in more elaborate QPLD docking of the six ligands shown in Fig. 1. Consequently, the consistent set of QPLD docking poses of unmodified Bcl2 proteins and BH1/BH3 domain analogue peptides allowed thorough comparison of the protein-ligand interaction profiles of all systems under study.

2.7. Peptide design

Based on the molecular docking Bcl2/ligand interaction profiles, we determined the amino acids (AAs) important for ABT263 and Hyp interactions within BH1 and BH3 domains of Bcl2 protein (yellow and orange marked sequences in Fig. 4B). Based on these sequences, we designed BH1 (26AA) and BH3 (24AA) domain peptides (sequences in Fig. 5A) of wild type sequence wBH1 and wBH3, and of scrambled sequence scBH1 and scBH3 (Fig. 5B and C). In scBH1 and scBH3 scrambled sequences, we changed AAs important for ligand interaction to alanines (Fig. 5B and C). Peptides were custom made by GeneCust (France) in HPLC purity (≥80%).

2.8. Fluorescence spectra measurements

Fluorescence spectra measurements were performed by a spectrofluorometer (RF-5301 PC, Shimadzu, Japan) at room temperature. We used the 280 and 274 nm excitation wavelengths to excite the tryptophan (W) and tyrosine (Y) intrinsic fluorescence, respectively. Emissions of W and Y fluorescence were recorded at wavelength from 300 to 700 nm using 5 and 10 nm emission and excitation bandwidths.

Measurements were carried out in either DMSO or phosphate buffered saline solution (PBS) (pH 7.4) with 0.04% Pluronic®F127 (Sigma Aldrich, Slovakia). Peptide stock solutions were prepared in DMSO at 2 mM concentration. The final concentration of peptides (WBH1, SBH1r, WBH3 and SBH3r) was kept constant at 1 μM in all measurements. The binding ligands ABT263 or Hyp were added in following concentrations (100 nM, 500 nM, 1μM, 5μM and 10 μM). Fluorescence signals were analyzed by Origine software (OrigineLab, USA).

2.9. Microscale thermophoresis

Microscale thermophoresis (MST) is a technique that allows differentiation between bound and unbound molecule states based on a molecule´s physical parameters (size, charge and conformation). MST uses an optical approach, fluorescence measurement of either covalently attached or intrinsic fluorophores in biomolecules, to characterize their properties such as protein-protein interactions, small molecule binding, enzyme kinetics etc. in free solution and with low sample consumption [70,71].

MST measurement detects the change in fluorophore fluorescence intensity as the molecules move across temperature gradients in water-based environment. Fluorescence change has two components, first is a function of temperature change (temperature-related intensity change, TRIC), and the second is a function of concentration change during molecules´ movement across the temperature gradient (thermophoresis). During a temperature change ΔT, both components, TRIC and thermophoresis, contribute to the measured MST signal as follows [72]

$$\frac{\partial}{\partial T}(cF) = c\frac{\partial F}{\partial T} + F\frac{\partial c}{\partial T} \quad (1)$$

The first term of the equation refers to fluorescence intensity change upon temperature (TRIC), whereas the second term is related to the concentration change due to thermophoresis along a spatial temperature gradient. Both signals are additive and contribute to the measured overall shift in fluorescence.

In practice, MST measurement is conducted by heating a small volume of a solution of the fluorescent molecule (target) with an infrared (IR) laser. Water molecules strongly absorb the infrared radiation, which generates a rapid controllable change in temperature that induces both TRIC and thermophoresis. Both signals result in a quantifiable fluorescence change that is not only a function of the applied temperature but also of the interaction with an unlabeled ligand. The MST instrument excites and records fluorescence within the sample before, during and after the IR-laser is turned on. The relative fluorescence is used to quantify the ligand binding:

$$F_{norm} = \frac{F_1}{F_0} \quad (2)$$

Where F_{norm} is normalized fluorescence; F_1 is fluorescence after diffusion across temperature gradient, and F_0 is initial fluorescence. F1 refers to the fluorescence measured several seconds after the IR-laser has been turned on, when the traces of unbound and bound state can be discriminated. Affinity is quantified by analyzing the change in F_{norm} as a function of the concentration of the titrated binding partner. As the thermophoretic movement of bound and unbound state superpose linearly, the fraction bound (FB) is described by:

$$F_{norm} = (1-FB)F_{norm,unbound} + (FB)F_{norm,\,bound} \quad (3)$$

Where FB is fraction bound; $F_{norm,\,unbound}$ is normalized fluorescence of the unbound state; $F_{norm,\,bound}$ is normalized fluorescence of the bound state [70,71].

Our MST measurements were performed on a Monolith NT.LabelFree instrument (NanoTemper Technologies GmbH) using the BH1 peptide intrinsic fluorescent signal from tryptophan (W). We used 280 nm excitation and 360 nm emission wavelengths to excite and detect the W intrinsic fluorescence. Monolith NT.LabelFree settings were MST power = 40%; LED power = 60%. Measurements were carried out in PBS (pH 7.4) with 0.04% (v/v) Pluronic®F127 (Sigma Aldrich, Slovakia) in hydrophobic capillaries (NT.LabelFree capillaries, NanoTemper Technologies GmbH). The concentration of WBH1 or SBH1r peptides was kept constant at 1 μM. The unlabeled binding partner ABT263 or Hyp were titrated in 1:1 serial dilution. The highest concentration of ligand was 100 μM and 200 μM for ABT263 and Hyp, respectively. The data were analyzed and fitted by MST analysis software NT Control and MO AfinityAnalysis, respectively (NanoTemper Technologies). The dissociation constant was then determined using a single-site model to fit the curve.

2.10. Statistical analysis

Experiments under all conditions were done in at least three independent repetitions. Statistical analysis was carried out by either Student's *t*-test or ANOVA using SigmaPlot (Ver. 12.0). A $p < 0.05$ was considered significant.

3. Results and discussion

3.1. Hyp and ABT263 effects on the Bcl2 protein distribution and cell viability

The malignant U87 MG and nonmalignant HCAEC cells express proteins of the Bcl2 family including Bcl2, Bcl_{XL}, Mcl1, Bax and Bak [73–75]. Recently, we have demonstrated that Hyp treatment of U87 MG and HCAEC cells affected Bcl2 proteins synthesis and distribution (Bax, Bak, and Bcl2) [37,76,77]. The mechanisms underlying Hyp effect on Bcl2 proteins distribution are still elusive. However, BH3 mimetic molecules functioning as inhibitors of anti-apoptotic Bcl2 proteins (Bcl2, Bcl_{XL} and Mcl1) have been shown to affect Bcl2 expression levels and initiate translocation and activation of Bax [19,78–80]

This led us to the hypothesis that Hyp may also act as Bcl2 inhibitor. First, we compared the effects of Hyp and a specific Bcl2 inhibitor, ABT263 [25]; Davids and Letai 2012; [20] on the Bcl2 protein distributions in U87 MG and HCAEC cells.

In control U87 MG and HAEC cells, Bcl2 protein distribution was in the distinct foci (Fig. 2Aa and Ac). Previously, we have shown by mitochondria specific staining with MitoTrackerOrange that the foci were localized at mitochondria or at contact sites between ER and mitochondria [40,81]. Observed Bcl2 distribution in U87 MG and HAEC control cells corresponded well with known distributions in various types of cells [38–42]. In control U87 MG cells, the Bcl2 signal was also present in the nuclei, which we did not see in HCAEC cells (Fig. 2Aa**)**. The presence of Bcl2 in nuclei is typical of malignant cell lines [82–87].

24 h incubation with Hyp in either U87 MG or HCAEC resulted in significant changes in the Bcl2 distribution patterns. There was a striking Bcl2 translocation into nuclei and a corresponding decrease of Bcl2 signal in foci outside of the nucleus in both U87 MG and HAEC cells (Fig. 2Ab and Ad). Hyp effect on Bcl2 distribution is time and concentration dependent (Fig. 2).

The ABT263 presence in either U87 MG or HCAEC cells resulted in a similar effect at 1 h and 6 h incubations (Fig. 2B**)**, where Bcl2 translocated from mitochondria into nucleus, and the effect was time and concentration dependent. Fig. 2B shows the results obtained in U87 MG cells, but we observed similar results in HCAEC cells (data not shown).

The presence of Bcl2 in nuclei strongly correlates with the cell cycle in the various types of malignant cells such as breast, colorectal, myeloma, leukemia, lymphoma, prostate, cervical and lung cancer lines [82–87]. The relatively strong Bcl2 expression in nuclei during mitosis suggests that Bcl2 may protect the malignant cells from apoptosis occurring during mitosis, and play a role in cell immortalization [82]. Further, there is strong evidence that Bcl2 presence in the nuclei play a role in genomic instability and development of cancer by suppressing DNA repair by interaction with KU70 and KU80 proteins [86–88]. On

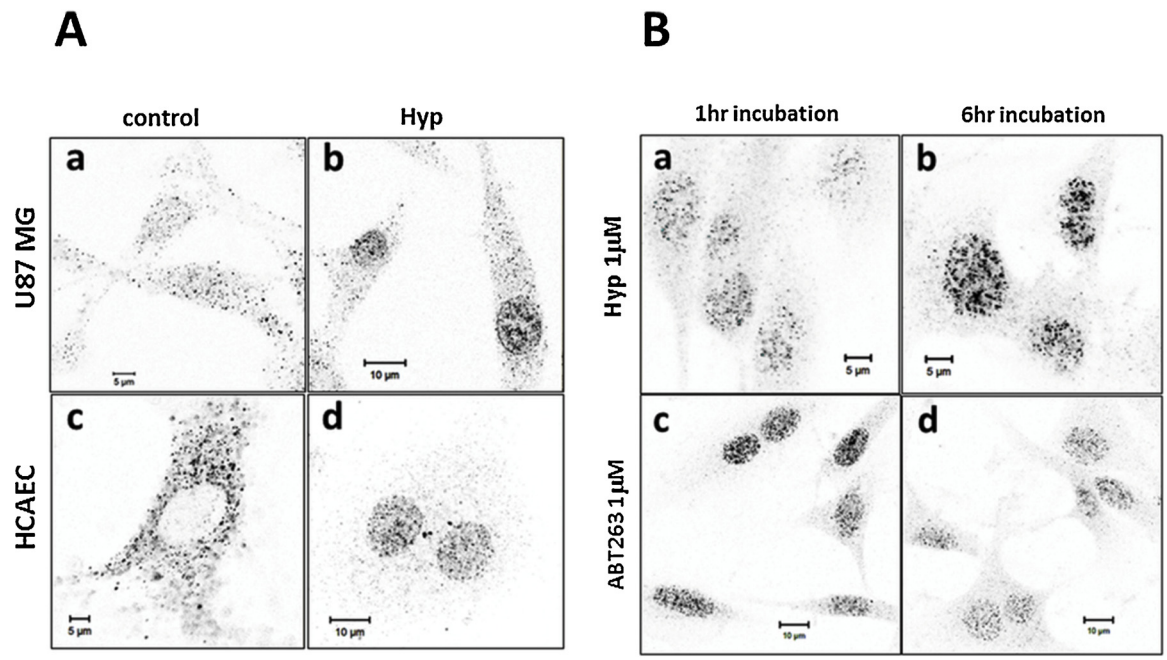

Fig. 2. Hypericin without illumination induces Bcl2 translocation to nucleus similar to the BH3 mimetic ABT 263. (A) Figure shows Bcl2 distribution in the absence **(Aa** and **c)**, and in the presence **(Ab** and **d)** of 500 nM Hyp (24 h incubation) in U87 MG and HCAEC cells. **(B)** Figure shows Bcl2 distribution in U87 MG cells in the presence of either 1μM Hyp (**Ba** and **b**) or 1μM ABT263 (**Bc** and **d**) (at 1 and 6 h incubations). The scale bars correspond to 5 and 10 μm.

the other hand, Bcl2 translocation into nuclei upon a variety of cell treatments was associated with on-set of apoptosis [85,89,90].

High expression levels of anti-apoptotic proteins including Bcl2 and dysregulation of Bcl2 phosphorylation is a hallmark of certain cancer types [78,91,92]. It has been shown that Bcl2 phosphorylation at multiple phosphorylation sites is necessary for its full anti-apoptotic potential. Specifically, Bcl2 phosphorylation at Ser70 by protein kinase Cα (PKCα) stabilizes Bax binding to Bcl2, and protects Bcl2 against proteolytic degradation [92,93]. Previously, we found that in U87 MG cells the Bcl2 protein was phosphorylated at Ser70 (pBcl2S70) and co-localized with PKCα [81]. Interestingly, the presence of Hyp increased the Bcl2/PKCα co-localization and the translocation of pBcl2S70 into nucleus [77].

In the next step, we studied the effects of ABT263 on cell viability (Fig. 3) in U87 MG and HCAEC. Fig. 3 shows the ABT263 effect on cell viability at three different concentrations (0.5, 1, and 10 μM) and incubation times (1, 6, and 24 h) in U87 MG (Fig. 3A) and HCAEC (Fig. 3B) cells. In U87 MG cells, ABT263 resulted in a small decrease of 10–20% in cell viability after 1 and 6 h incubation in comparison to control cells, however, this effect was overturned after 24 h incubation (Fig. 3A).

In contrast, HCAEC cells incubations at 6 and 24 h resulted in concentration and time dependent decrease in cell viability (Fig. 3B) in comparison with control cells. In 6 h incubation, ABT263 caused significant decrease in cell viability of 87% and 73% at 1 and 10 μM concentrations, respectively. In 24 h incubation, the effect was more prominent with decrease in viability of 75%, 59% and 0% at 0.5, 1 and 10 μM concentrations, respectively.

In the comprehensive study of ABT263 biological effects [25], the authors investigated a panel of human tumor cell lines and identified ABT263 sensitive and resistant cell lines. The decrease in U87 MG cell viability did not have noticeable concentration dependence up to 10 μM, indicating U87 MG resistance to the ABT263. The viability decrease seen in HCAEC is, on the other hand, symptomatic of ABT263 sensitive

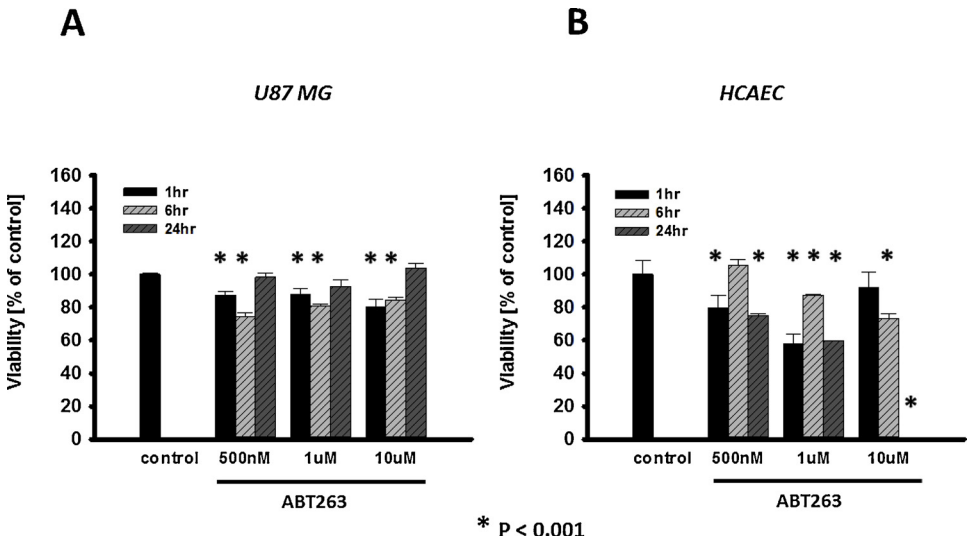

Fig. 3. Concentration and time-dependent effect of ABT263 on cell viability. Survival rate of U87 MG (**A**) and HCAEC (**B**) cells treated with ABT263 at various concentrations and incubation times. Experiments under all conditions were done in at least three independent repetitions. Statistical analysis was carried out by Student's *t*-test.

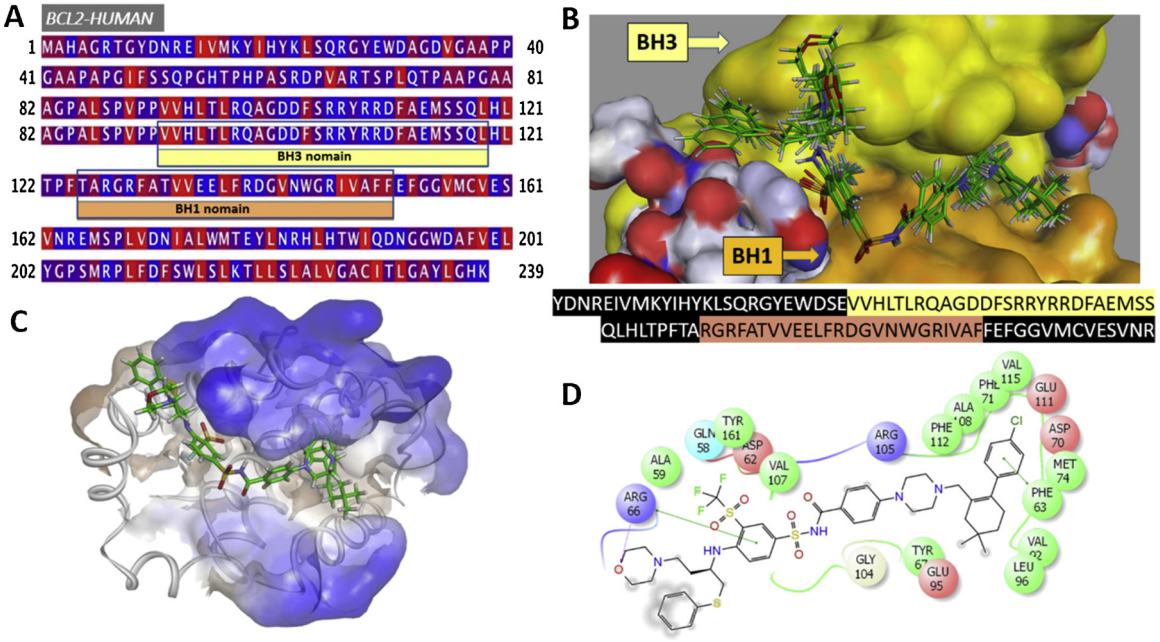

Fig. 4. BH3 and BH1 domains of the Bcl2 protein and protein-ligand interactions. A) Bcl2 protein amino acid sequence visualized in Jalview with amino acid color coding according hydrophobicity. The BH3 and BH1 are highlighted in yellow and orange,respectively. **B)** ABT263 (carbon atoms in green) docked into Bcl2 (PDB code 4IEH) together with the 4IEH sequence colored according BH3 and BH1 domains. **C)** ABT263 conformations (with docking score below 1.5 kcal/mol) matching the shape of the binding site of Bcl2. The molecular surface of the BH3 and BH1 domains shows hydrophobicity in blue. **D)** Detailed interaction profile of the ABT263 conformation corresponding to the best binding energy.

cell lines [25].

Previously, others and we have shown that incubation of U87 MG cells with Hyp up to 24 h did not significantly affect cell viability in comparison with control cells [81,94,95]. In contrast, we observed that 24 h incubation of HCAEC cells with Hyp has a significant cytotoxic effect [37] where Hyp caused a decrease of healthy cell population to 50%.

The ABT263 effect on U87 MG and HCAEC viability seems to emulate the Hyp effect in these cells, which we have shown previously [37,81,95]. Hyp presence itself did not significantly affect the U87 MG viability during 1–24 hr incubation, but HCAEC cells were susceptible to Hyp treatment. The 24 h incubation with 0.5μM Hyp led to decrease of HCAEC viability to 50% [37].

Taking together Bcl2 distribution patterns and viability data, our results show that Hyp may act via a Bcl2 dependent mechanism. Previously, we have shown that Hyp affects Bcl2 proteins distribution and triggered translocation of Bax to mitochondria [37,76]. Hyp downregulated Bcl2 expression level of total and phosphorylated (at serine 70) protein [37,77]. Further, we have demonstrated that Hyp presence resulted in additional effects such as increased oxidative stress, increased autophosphorylation of pro-apoptotic pKCδ, swollen Golgi apparatus and fragmentation of ER [37,77].

Our results are in good agreement with observations, where various BH3 mimetics including ABT263 and gossypol have been shown to downregulate Bcl2 expression levels and initiate translocation and activation of Bax [19,78–80,96]. Further, many BH3 mimetics, including ABT737, gossypol, and obatoclax also show off-targets effects such as ER stress, increased oxidative stress and induction of autophagy [26,97].

The difference between U87 MG and HCAEC cells sensitivity towards Hyp and ABT263 may reside in upregulation of Mcl1, an anti-apoptotic member of Bcl2 family. It has been shown that various Bcl2/Bcl_{XL} inhibitors, including ABT263, upregulated Mcl1 in malignant cells and render them resistant to these compounds [98–100]. The upregulated Mcl1 can also inhibit an autophagy. In cancer cells, autophagy can augment apoptosis triggered by Bcl2 inhibitors [26,101]. The anti-apoptotic Bcl-2 family members Bcl2, Bcl_{XL} and Mcl1 can form a complex with Atg6/Beclin1 and prevent it from forming a multiprotein complex essential for the early steps in autophagy. It was shown that knockdown of Beclin1 and Atg5 in U87, U343, and MZ-54 cells greatly diminished the extent of cell death induced by (−)-gossypol [26].

3.2. *Bcl2 protein-ligand interactions*

Our *in vitro* findings indicated that Hyp may act via a Bcl2 dependent mechanism. One possibility is a direct ligand-protein interaction. The Hyp interactions with its known interacting partners are predominantly hydrophobic [54–58].

Structural analysis of pro-survival Bcl2 family members revealed a characteristic hydrophobic pocket encompassing BH1-BH3 domains, which acts as a receptor for the interacting partners [1]. This hydrophobic pocket binds BH3 mimetics, including ABT737 or ABT263 (Fig. 4), selective Bcl2/Bcl_{XL} inhibitors [18,22].

Considering all this led us to hypothesis that Hyp may interact with Bcl2 via hydrophobic pocket similarly to known Bcl2 inhibitor ABT263.

We obtained the human Bcl2 sequence from UniProt database (https://www.uniprot.org/uniprot/P10415#sequences) and visualized by Jalview software [102] (Fig. 4A). The corresponding PDB sequence search revealed availability of several Bcl2 protein structures (either X-ray or NMR). We selected 4IEH PDB structure [63] for our introductory docking studies. The ABT263 docking results are summarized in Fig. 4B-D. The BH1 and BH3 domains are highlighted in orange and yellow, respectively (Fig. 4B). We hypothesized that it may also be an interaction site for Hyp and tested this prediction by modeling approach and by *in vitro* experiments.

The comparison of ABT263 and Hyp conformational sampling (Fig. 1) with other BH3 mimetics revealed that ABT263 is the most flexible molecule of the analyzed set. The ABT263 QPLD results indicate that due to conformational flexibility ABT263 adapts well to the protein-binding site as illustrated in Fig. 4B. In contrast, Hyp conformation is quite restricted with small freedom of the hydroxyl groups. Despite the rigidity caused by electron delocalization of the phenyl

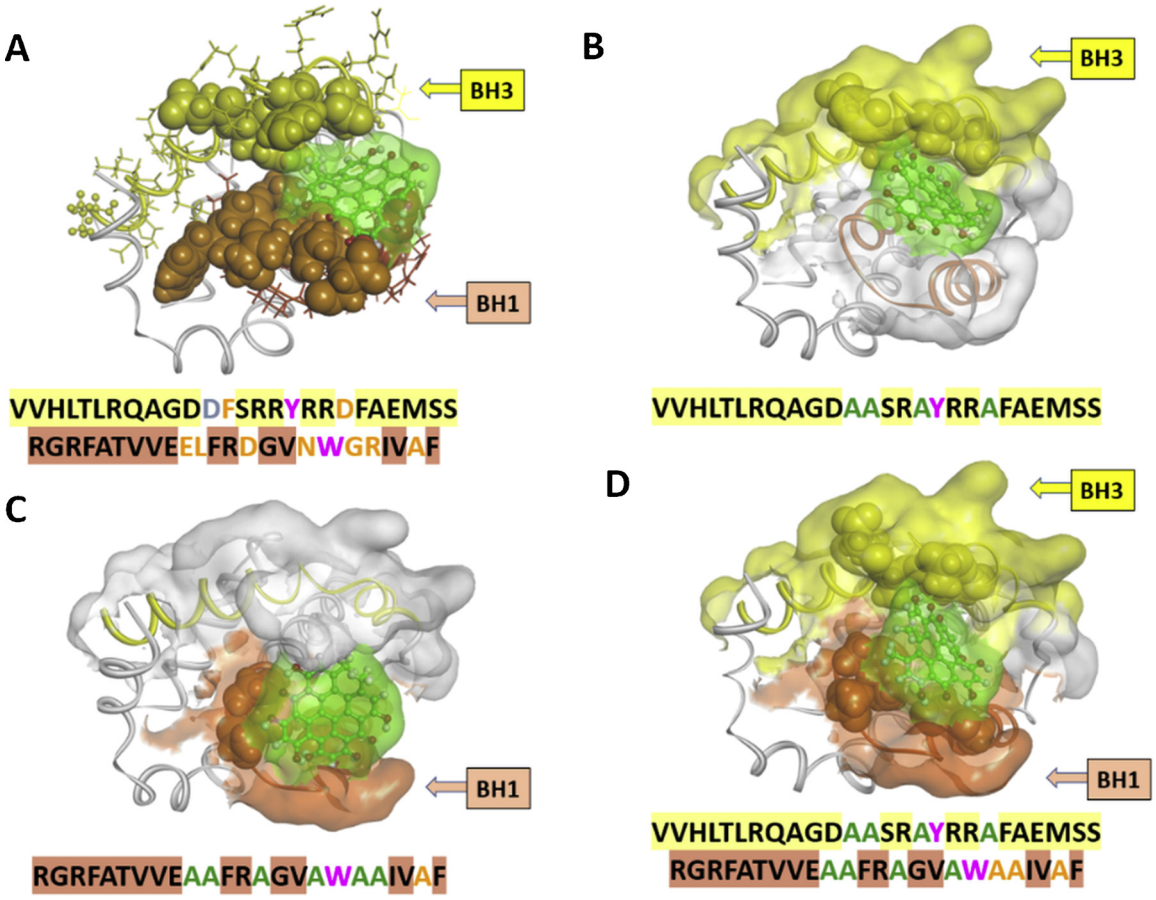

Fig. 5. ***In silico*** **Bcl2 mutations and Hyp binding. A)** The wild type Bcl2 protein-ligand interactions. The BH3 domain is colored yellow, while the BH1 domain orange.Ball and stick representation is used for the first domain amino acid; the amino acids selected for mutation are shown in CPK representation. **B)** *In silico* mutation of the BH3 domain (yellow coloring of the semitransparent soft surface) and Hyp binding (ball and stick representation with green-colored carbons; semitransparent grey-colored molecular surface). **C)** *In silico* mutation of the BH1 domain (orangecoloring of the surface) and Hyp binding. **D)** *In silico* mutation of domains, the BH1 and BH3, and Hyp binding.

rings, the molecule can bind quite well to the BH1-BH3 domain hydrophobic residues in the Bcl2, as shown in Fig. 5A.

In order to determine the importance of amino acids for binding both ligand molecules, ABT263 and Hyp, within the BH1 and BH3 domains of Bcl2 protein, we performed "*in silico*" site directed amino acid mutations in the BH1 and BH3 domains as the next step. We have mutated the AAs important for both ligands binding to alanine (Fig. 5B and C). We were interested to see how ABT263 and Hyp will bind to the mutated proteins (Fig. 5B-D).

Table 1 summarizes the comparison of ABT263 and Hyp docking energies to the wild type and computer modeling mutated Bcl2 protein. Based on relative ligand binding energies, our modeling experiments predicted that mutations did not improve the ABT263 binding. In the case of Hyp, the BH1 mutation and the simultaneous BH1 and BH3 mutations predicted improved ligand binding. Fig. 5(B, C and D) shows the corresponding position of Hyp within the three *in silico* mutated Bcl2 proteins.

Table 1
Comparison of relative ligand binding energies for wild type and *in silico* mutated Bcl2 proteins.

Protein	ΔE [kcal/mol]	
	ABT263	Hyp
Bcl2*	0	1.28
Bcl2/BH1 mut	0.83	0
Bcl2/BH3 mut	5.52	2.4
Bcl2/BH1 & BH3 mut	1.16	0.38

* See Table 3 for absolute QPLD docking energies of Bcl2 wild-type protein.

The modeling data (Figs. 4 and 5) illustrated the possibility for competitive binding of ABT263 and Hyp and suggested that Hyp can bind into the Bcl2 hydrophobic groove and cause similar effects as Bcl2 known inhibitor ABT263.

We designed four small peptides to confirm our molecular modelling results and to test the importance of the BH1/BH3 amino acids for Bcl2 ligand binding in experiment. Two peptides were of wild type (w) and two contained alanine mutated (scrambled, sc) sequences corresponding to BH1 and BH3 domains of Bcl2 (Fig. 6). More than one hundred conformations were obtained for all peptides from http://bioserv.rpbs.univ-paris-diderot.fr/services/PEP-FOLD3/. In scBH1 and scBH3 sequences, we replaced AAs important for ligand interaction with alanine same as in *in silico* approach. Fig. 6 illustrates the superposition of all thus modelled structures.

3.3. Hyp and ABT263 alike quench the endogenous fluorescence of tryptophan and tyrosine in Bcl2 peptides

To confirm that Hyp may bind to the BH1-BH3 hydrophobic pocket of Bcl2 protein, we used BH1 and BH3 domain peptides of wild type and scrambled sequences in fluorescence spectra measurements (Figs. 5 and 6).

The fluorescent properties of naturally occurring fluorescent amino acids phenylalanine, tyrosine and tryptophan are often used to study

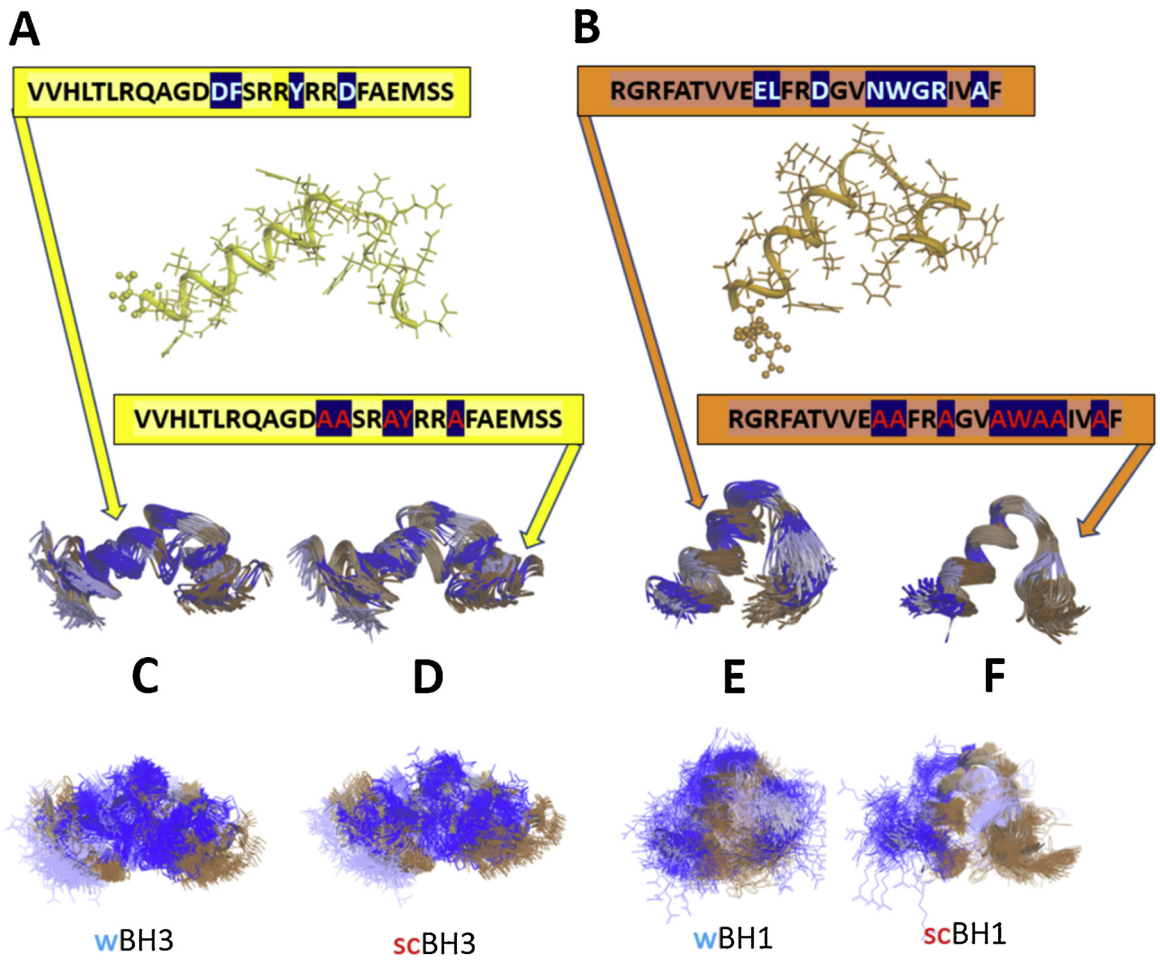

Fig. 6. Hydrophobicity model of the BH1 and BH3 peptides. **A)** BH3 and **B)** BH1 domain analogs of Bcl2. Biovia DS visualizer was used to create these images. Ribbon (top) and all-atom (bottom) visualization of the peptides derived from Bcl2 (PDB code 4IEH). Around 100 conformations were built and optimized for each of the four peptides. More intensive blue color corresponds to the highest hydrophobicity residues. **C)** and **E)** show the superposition of the wild type peptide conformations; **D)** and **F)** of the scrambled peptide conformations.

protein structure function properties. The tryptophan (W) is exploited the most often because it has a high fluorescence quantum yield, its fluorescent properties (emission wavelength, Stokes shift, lifetime) depend on local environment, and its fluorescence can be quenched or modified by neighboring AA side chains, hydrogen bonds, by polarity of solvent or by interaction with other molecules and ions [103–105]. The tyrosine (Y) is used to a lesser extent than W, mainly because it has low quantum yield and low sensitivity to the local environment [106–108]. However, despite its shortcomings, Y is exploited to study the protein folding and unfolding, interaction of peptides and proteins with lipid membranes, and conformational changes of intrinsically disorder proteins [106–109].

Both, BH1 and BH3 peptides contain endogenous fluorescent amino acid, tryptophan (W18) and tyrosine (Y17), respectively (Fig. 5). We used the fluorescent properties of W18 and Y17 residues, respectively, to study interaction of BH1 and BH3 peptides with Hyp and ABT263. Based on the amino acid sequence, all sequenced peptides display moderate to high hydrophobicity (35–70%) (Fig. 6C-D).

Fig. 7 shows the fluorescence emission spectra of BH1 and BH3 peptides of wild type and scrambled sequences in nonpolar solvent DMSO. Peptides were dissolved in DMSO at the final concentration of 1μM. The wBH1 and scBH1 spectra (Fig. 7 left upper and lower panels) were recorded within 300–500 nm range with 280 nm excitation wavelength. The wBH3 and scBH3 spectra (Fig. 7 right upper and lower panels) were recorded within 300–500 nm range with 274 nm excitation wavelength. Peptide spectra were measured in the absence and presence of ligands ABT263 and Hyp at the 1μM final concentration. The wBH1 and scBH1 spectra in the absence of ligands display maximum intensity at 342 and 343 nm, respectively. These values correspond well with a typical tryptophan (W) maximum intensity in nonpolar environment [104]. The scBH1 fluorescent maximum intensity was 1.7 fold higher than that of wBH1, indicating that W18 fluorescence in wBH1 was probably quenched by carbonyl groups of neighboring amino acids asparagine (N17) and glutamine (G19) [103,107,110]. In the presence of 1 μM ABT263 (Fig. 7, red dash dot line), there was no change in the wBH1 spectrum, but the scBH1 spectrum displayed a slight increase in fluorescence maximum intensity, which can indicate either stabilized peptide structure upon ligand binding, or the possibility of ligand binding sites on a different side of the peptide chain.

Increased ABT263 concentration (at 5 and 10 μM) resulted in decreased fluorescence maximum intensity in inversely proportioned manner in both wBH1 and scBH1 spectra, which are available in supplementary **Fig. S1**, suggesting that ABT263 binds to both peptides. The presence of 1μM Hyp (Fig. 7, green dotted line) caused a decrease of fluorescence maximum intensity in wBH1 spectrum, but no change in scBH1, indicating that Hyp binds to BH1 peptide, and binding is stronger to wBH1 than to scBH1. The wBH1 spectra also indicate that Hyp binds stronger than ABT263. The scBH1 spectra slight increase in the presence of ABT263 may indicate peptide stronger interaction with ABT263 than with Hyp.

The wBH3 and scBH3 spectra in the absence of ligands (Fig. 7 right

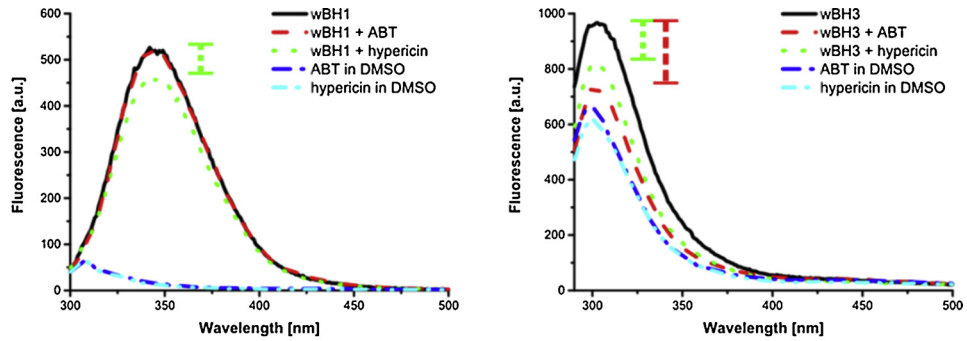

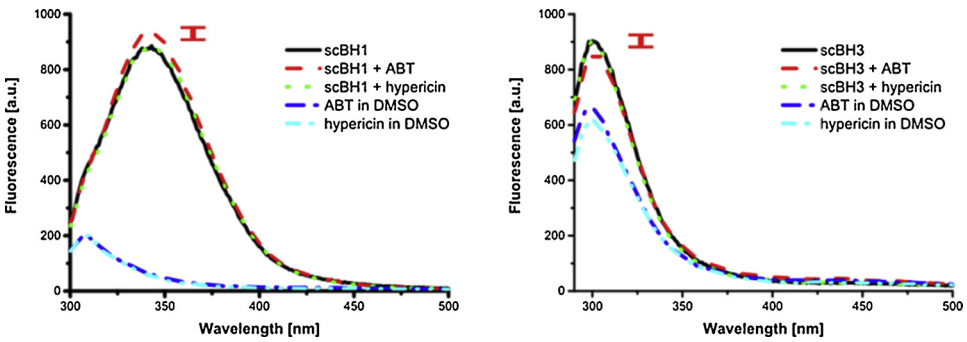

Fig. 7. Hyp and ABT263 alike decrease endogenous fluorescence of tryptophan (W) and tyrosine (Y) in Bcl2 peptides. Fluorescence spectra of wBH1, scBH1, wBH3 and scBH3 peptides (1μM) in the absence (blackline) and presence of Hyp (green dotted line) and ABT263 (red dashed line) in DMSO solutions. Fluorescence signals from Hyp (cyan dash-dot-dotted line) and ABT263 (blue dash-dotted line) alone in DMSO. Markers demonstrate fluorescence quenching of tryptophan (BH1) and tyrosine (BH3) in the presence of hypericin and ABT.

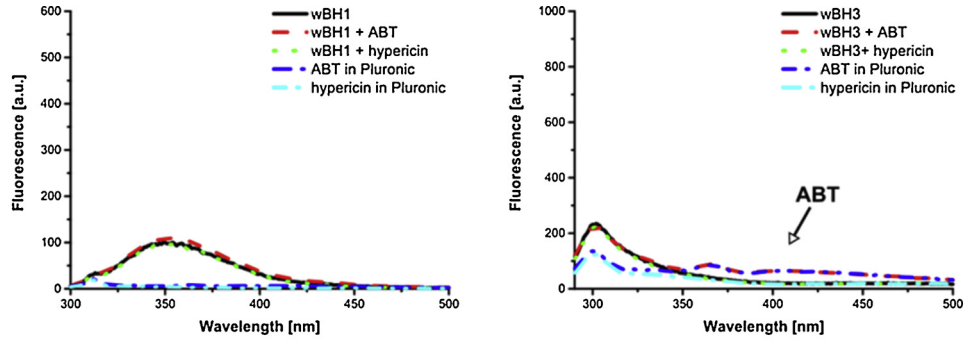

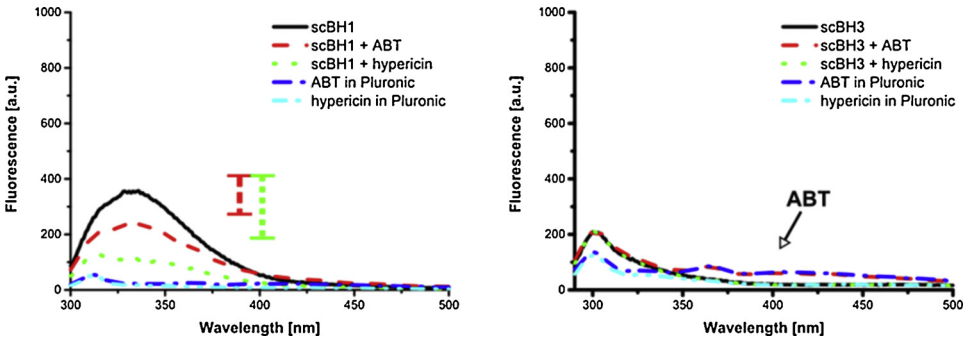

Fig. 8. Hyp and ABT263 fluorescence quenching in BH domain peptides depends on solvent polarity. Fluorescence spectra of wBH1, scBH1, wBH3 and scBH3 (1μM) in the absence (blackline) and presence of hypericin (green dotted line) and ABT (red dashed line) in PBS (pH 7.4). Fluorescence signals from Hypericin (cyan dash-dot-dotted line) and ABT (blue dash-dotted line) only were detected in PBS(pH 7.4) with 0.04% Pluronic. Markers demonstrate fluorescence quenching of W18(BH1) and Y17(BH3) in the presence of hypericin and ABT.

upper and lower panels) display maximum intensity at 303 and 300 nm, respectively. The maxima values correspond well to a typical tyrosine (Y) maximum intensity [106,107,111,112]. The fluorescent maximum intensity did not differ between wBH3 and scBH3 spectra reflecting the fact that Y17 fluorescence has low sensitivity to changes in the surrounding environment [108,109]. In the presence of either ligand ABT263 (Fig. 7, red dash dot line) or Hyp (Fig. 7, green dotted line) at 1 μM concentration, there was a significant decrease in fluorescence maximum intensity of wBH3 spectra, with a stronger effect in the presence of ABT263. These findings indicate that both ligands bind to wBH3 peptide. The scBH3 spectra in the presence of Hyp displayed no change in fluorescence maximum intensity and slight decrease in the presence of ABT263, indicating that bot ligands have weaker binding than in wBH3.

Fig. 8 shows the fluorescence emission spectra of BH1 and BH3 peptides in polar solvent of phosphate buffered saline solution (PBS) at physiological pH (7.4) with 0.04% Pluronic®F127. Pluronic®F127 was added to improve solubility of hydrophobic peptides in polar solvent. The BH1 and BH3 peptide spectra were recorded within 300–500 nm range with 280 and 274 nm excitation wavelengths, respectively. Peptides and ligands (ABT263 and Hyp) were first dissolved in DMSO at the 2 mM concentration each, and then diluted in PBS with 0.04% Pluronic®F127 at final concentration of 1μM. Concentration of DMSO was kept at less than 0.01%.

The wBH1 and scBH1 spectra (Fig. 8 left upper and lower panels) in the absence of ligands display maximum intensity at 354 and 336 nm,

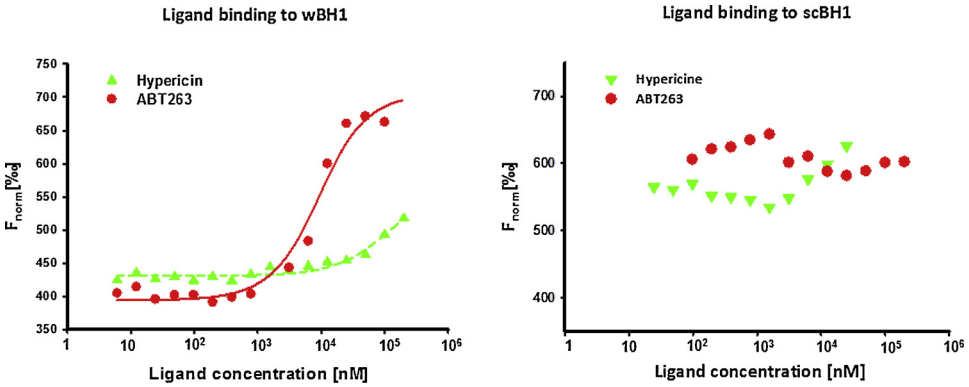

Fig. 9. Determination of Hyp binding to BH1 peptides by MST. Plot of the BH1 peptide normalized fluorescence F_{norm} (‰) vs. the concentration of ligands, ABT263 (red symbols) and Hyp (green symbols) from MST experiments. Fraction bound plot of the MST experiments shows ligands binding to wBH1 (left panel) and scBH1 (right panel) peptides in PBS (pH 7.4) with 0.04% (v/v) Pluronic®F127. Lines represent fits of the changes in thermophoresis signal data points, and yielded K_D of 6.75 ± 0.02 μM and 118.72 ± 0.01 μM for ABT263 and Hyp binding to wBH1, respectively.

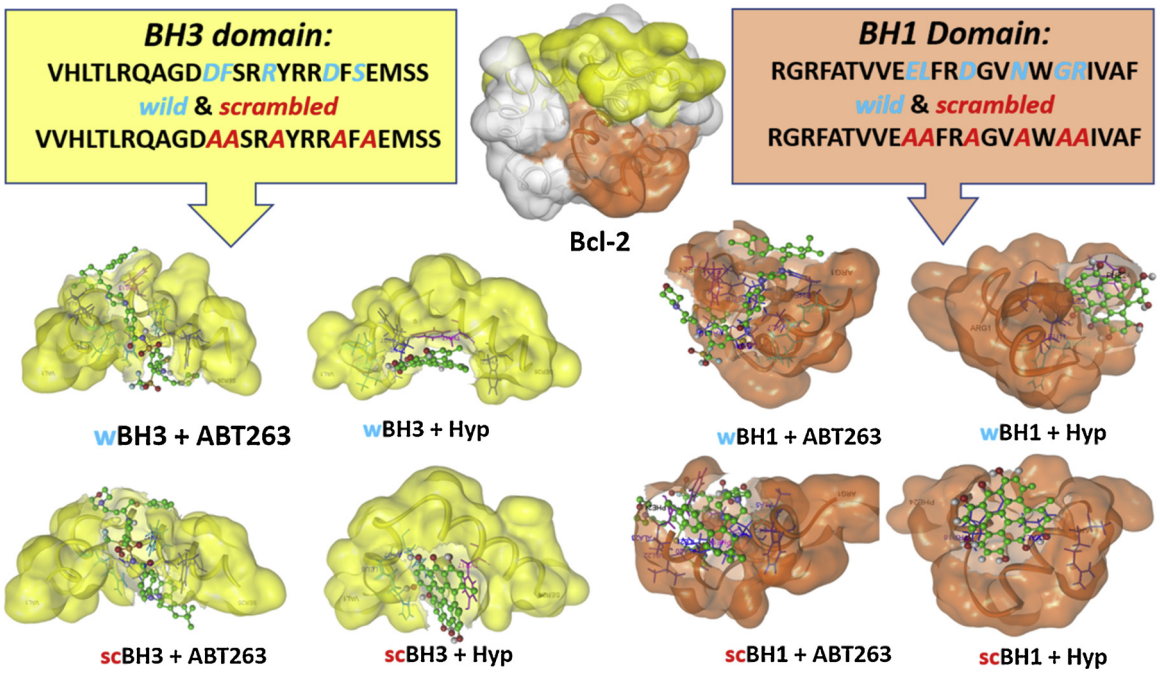

Fig. 10. Prediction of Hyp and ABT263 binding to BH peptides. BH1 (orange)and BH3 (yellow) domains of Bcl2 protein (PDB code 4IEH) and their sequences. The corresponding structures of *wild* and *scrambled* peptides are shown as molecular surfaces. Docking results of ABT263 and Hyp into the binding site of the four peptides are shown. Their detailed interaction profiles are illustrated in **Fig. S2** in Supplementary Materials.

Table 2
QPLD docking (docking score in kcal/mol) of BH3 mimetics and Hyp to the BH1 and BH3 peptides.

	ABT199	ABT263	ABT737	Gossypol	Hyp	TW37
wBH1	−4.31	−4.35	−4.89	−6.68	−6.17	−5.63
scBH1	−3.59	−4.43	−5.01	−4.70	−3.21	−5.47
wBH3	−4.45	−4.23	−3.71	−5.66	−4.94	−4.53
scBH3	−3.84	−3.40	−4.38	−4.38	−2.87	−2.42

respectively. Both, wBH1 and scBH1 spectra measured in PBS with 0.04% Pluronic®F127 displayed the fluorescence maximum intensity decrease by 4.7 fold and 2.3 fold, respectively, in comparison with spectra measured in DMSO (Fig. 7). In the case of wBH1 peptide spectra, the observed red shift of λ_{max} to 354 nm and 4.7 fold decrease in intensity is most likely due to the polarity of the solvent and aggregation of the peptide in a polar environment. It is also an indication that W18 in wBH1 is residue fully exposed to the environment [105,107]. The presence of either ligand ABT263 or Hyp did not change wBH1 spectra in PBS with 0.04% Pluronic®F127. This could be due to several reasons. One, that in polar environment W18 had low fluorescence intensity and changes upon ligand binding were below detection level. Second, wBH1 peptide aggregated, or that there was no ligand binding.

In contrast, scBH1 spectra (Fig. 8) show blue shift in λ_{max} from 343 to 336 nm and 2.3 fold decrease of fluorescence intensity in comparison with spectra measured in DMSO (Fig. 7). The blue shift of λ_{max} in scBH1 spectra may be due to the fact that highly hydrophobic scBH1 peptide (~ 70% hydrophobic residues) in polar solvent assumes conformation in which W18 will be buried in a hydrophobic environment and less exposed than in DMSO, similar to tryptophan residues positioned in hydrophobic core of proteins [107]. However, scBH1 spectra displayed sufficient fluorescence that allowed us to observe significant decrease in W18 fluorescence intensity in the presence of both ligands, ABT263 and Hyp, with stronger effect in the Hyp presence. This indicates that both, ABT263 and Hyp, can bind to scBH1 in polar environment.

The wBH3 and scBH3 spectra measured in PBS with 0.04% Pluronic®F127 (Fig. 8 right upper and lower panels) displayed large 4.75 fold decrease in Y17 fluorescence intensity with no change in λ_{max}. It is known that Y fluorescence is not very sensitive to solvent polarity [107,108], therefore the decrease in Y17 signal in a polar solvent is most likely due to peptides´ aggregation as they both contain more than 36% of hydrophobic residues. We did not observe any changes in wBH3 and scBH3 spectra in the presence of ligands most likely due to peptide

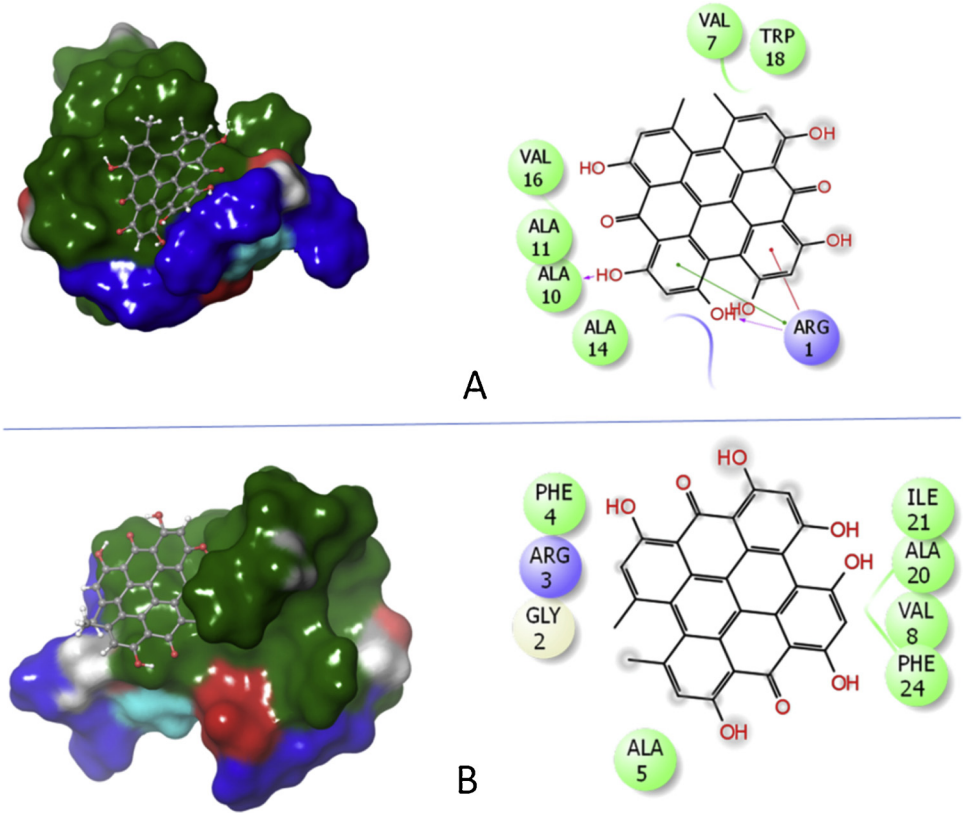

Fig. 11. Comparison of two equivalent binding positions and interaction profiles of Hyp to scBH1 peptide.
A) the lowest-energy binding position; **B)** binding on the opposite side of the peptide chain.The molecular surface of the peptide is colored according Maestro amino acid properties coloring scheme corresponding to hydrophobicity, charge and polarity, i.e.: **Dark green** - Hydrophobic (Ala, Cys, Ile, Leu, Met, Phe, Trp, Val, Pro); **Cyan -** Polar uncharged (Ser, Thr, His, Gln, Asn); **Blue** – Positives (Lys, Arg); **Red** – Negatives (Asp, Glu); **Gray** – Gly.

Table 3
QPLD docking results (docking score in kcal/mol) of Bcl proteins and BH3 mimetics including Hyp.

	ABT199	ABT263	ABT737	Gossypol	Hyp	TW37
Bcl2	−9.20	−9.09	−9.42	−6.17	−5.19	−8.20
Bcl_{XL}	−4.28	−4.98	−4.85	−5.72	−6.54	−6.44
Mcl1	−4.08	−3.69	−4.81	−4.77	−6.49	−6.10

aggregation. Another possibility is that because of low Y17 fluorescence intensity in PBS with 0.04% Pluronic, the changes in spectra upon ligand binding were below detection level.

Taking together all results from fluorescence spectra measurements, we have shown that the presence of both ligands, ABT263 and Hyp, decreased fluorescence signal of W18 and Y17 in wBH1 and wBH3 peptides, respectively. We have also demonstrated that AA mutation at the interaction site clearly affected interaction between peptides and ligands. Thus, our findings suggest that interaction of ABT263 and Hyp with peptides is feasible. It is known that ABT263 is an inhibitor Bcl2 protein and interacts with Bcl2 at the hydrophobic groove including BH3 and BH1 domains [18,113]. Therefore, our results indicated that Hyp indeed can interact with whole Bcl2 protein at the same hydrophobic pocket as ABT263.

3.4. Hyp and ABT263 bind to BH1 peptide

In order to identify and compare binding affinity of Hyp and ABT263 to BH1 and BH3 peptides, we used microscale thermophoresis measurements (MST). MST allows differentiating between bound and unbound states of molecules. MST uses fluorescence properties of either covalently attached or intrinsic fluorophores in molecules of interest to investigate their properties including protein-protein interactions and small molecule binding [70,71].

In our experiments, we exploited intrinsic fluorophores W18 and Y17 properties in BH peptides in MST label free measurements. MST technique detects the change in fluorescence intensity as molecule moves across temperature gradients in water-based environment, for which we have used PBS (pH 7.4) with 0.04% Pluronic. Due to low fluorescent signal of Y17 and BH3 peptides aggregation in PBS with 0.04% Pluronic, we were only able to measure ABT263 and Hyp binding to BH1 peptides by MST approach (Fig. 9). The concentration of wBH1 or scBH1 peptides was kept constant at 1μM, and ligands, ABT263 or Hyp, were titrated in 1:1 serial dilution. The titration resulted in a gradual fluorescence change due to thermophoresis, which was plotted as normalized fluorescence F_{norm} vs ligand concentration (Fig. 9) and fitted to obtain the binding constant. Fitting yielded a K_D of 6.75 ± 0.02μM and 118.72 ± 0.01 μM for ABT263 and Hyp binding to wBH1 peptide, respectively. Obtained MST measurements for scBH1 with ABT263 and Hyp did not yield suitable data for analysis.

Obtained K_D of 6.75μM for ABT263 binding to BH1 peptide is three orders of magnitude weaker than ABT263 binding to whole Bcl2 protein ($K_D \leq 1$ nM) [25,114]. BH1 peptide contains only part of Bcl2 interaction site and this may be one explanation of the differences in K_D values. In addition, both ligands, ABT263 and Hyp, are highly hydrophobic molecules and at concentrations ≥ 5μM in water-based environment form aggregates [114–117], which could have affected the MST measurements. To our knowledge, there is no information regarding Hyp binding to either BH peptides or whole Bcl2 protein.

3.5. Interaction profiles of BH1 and BH3 peptides with Hyp and other BH3 mimetics

The experiments with BH1 and BH3 peptides indicated that Hyp interacts more strongly with BH1 and weakly with BH3 peptide in comparison to ABT263. These findings prompt us to calculate the BH1 and BH3 peptides binding properties, and compare ABT263 and Hyp binding with other known BH3 mimetics.

The BH1 and BH3 fold modeling, as seen in Fig. 6, resulted in a variable set of a few hundred peptide conformations. The SiteMap

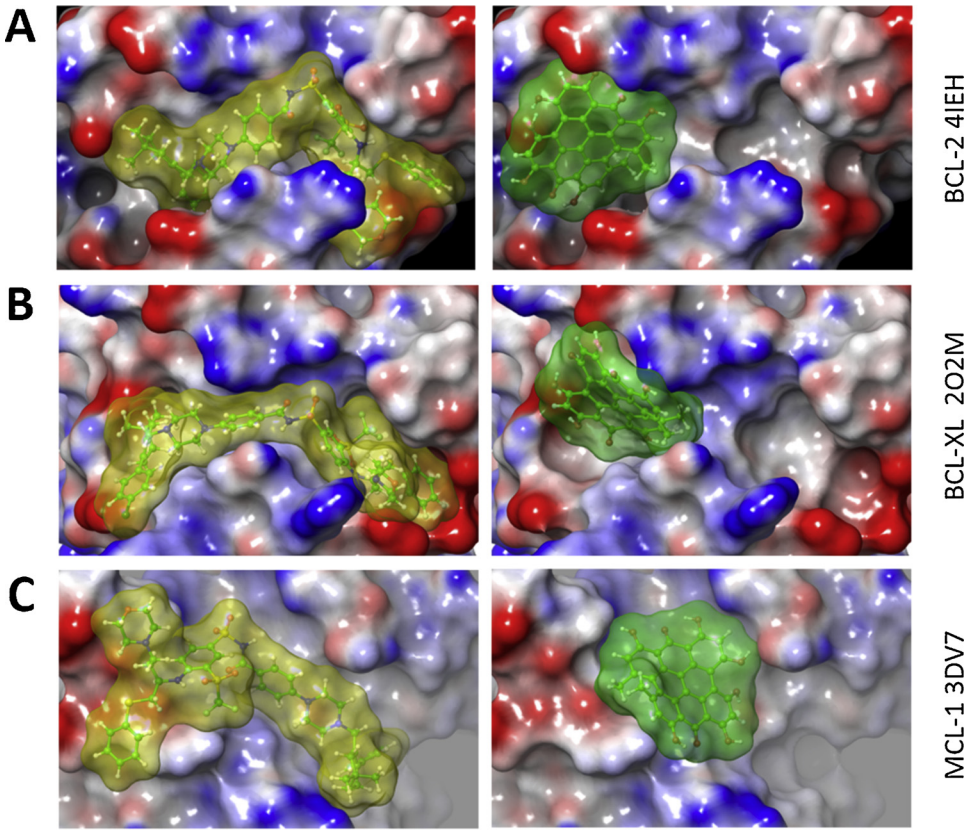

Fig. 12. Comparison of ABT263 (yellow semitransparent molecular surface) and Hyp binding (green semitransparent surface) to the selected members of Bcl2 family of proteins. **A)** Bcl2, **B)** Bcl_{XL} and **C)** Mcl1. The protein molecular surface is colored according the electrostatic potential (red for negative, blue for positive values). Glide docking results are presented on the pictures.

Table 4
Binding constants of selected BH3 mimetics.

K_D (nMol/L)	ABT263 [25]	Gossypol [118]	TW37 [119]
Bcl2	≤ 1.0	320	290
Bcl_{XL}	≤ 0.5	480	1110
Mcl1	550	180	260

program was used to predict their binding sites, and ABT263 or Hyp were docked into these sites (Fig. 10) using the Autodock VINA program. Fig. 10 shows the original Bcl2 protein surface with colored BH3 and BH1 domains in yellow and orange, respectively. Equivalent coloring was used for the wBH1, wBH3, scBH1 and scBH3, peptides, respectively. In addition, Fig. 10 displays the ABT263 and Hyp best docking configurations in BH1 and BH3 peptides. Detailed information regarding the peptide-ligand interaction profiles is available in supplementary **Fig. S2**. From the schematic color-coding of the intermolecular interaction profiles (green for hydrophobic, red and blue for charge/AA polarity) is apparent the dominance of the hydrophobic interactions between peptides and ligands. Other interactions, like hydrogen bonding, electrostatic interactions, $\pi-\pi$ stacking, etc. may also play important roles in stabilizing ligand binding in the protein/peptide binding sites.

The charge adjustments are better handled by the QPLD protocols. QPLD allows quantum chemical recalculation/adjustment of the atomistic charges on both, ligands as well as interacting amino acids. Such adjustment results in more elaborate calculation of the electrostatic interactions, hydrogen bonding, etc. In order to acquire superior docking results, we performed QPLD docking runs on BH1 and BH3 peptides. As a starting point, we used the best ABT263 and Hyp Autodock VINA peptide-ligand configuration. We have also compared Hyp docking to the other known BH3 mimetics. The resulting docking scores for wBH1, scBH1, wBH3, and scBH3 are summarized in Table 2. The corresponding docking results are visualized in **Figure S4.** The docking scores (Table 2) show that Hyp binds stronger to wBH1 than ABT263, which is in a good agreement with our data from fluorescence spectroscopy (Fig. 7). The rest of docking results also supports outcomes from fluorescence spectroscopy. The most important pattern to

Table 5
Chemo-informatics data, predicted LD_{50} values and reference EC_{50} values of selected BH3 mimetics and Hypericin.

Molecule	QuikProp [120] Calculated Values				Predicted data from http://tox.charite.de/protox_II [121]				EC_{50}(μMol/L) [25,26,32,37,119,122,123]		
	MW	donorHB	accHB	QPlogPo/w	Number of rotable bonds	Number of rings	Molec. Polar Surface Area	Predicted LD_{50}* (mg/kg)	Tumor cell lines	Endothelial cell lines	Ref.
ABT199	868.45	3	13	7.62	14	8	183.09	4000			
ABT263	974.61	1	16	8.25	18	7	170.42	560	0.1- 40.0		[25,122]
ABT737	813.43	2	13	7.53	17	6	164.49	2000			
Gossypol	504.45	2	5	3.23	5	4	155.52	325	8.0-30.0	2.2	[26,119]
Hyp	518.56	4	7	3.58	0	8	155.52	1000	0.1-10.0	0.5 - 1.0	[32,37]
TW37	573.70	3	8	5.48	9	4	132.31	5000	0.3-2.0	1.8	[119,123]

* All compounds belong to toxicity class IV (harmful if swallowed (300 < LD50 ≤ 2000) and V (harmful if swallowed (300 < LD50 ≤ 2000); none of the compounds belong to the predicted class VI (nontoxic). The four compounds in predicted class IV are highlighted.

stabilize all explored ligands into the BH peptides binding sites is predominance of the hydrophobic interactions. Such interaction patterns are visualized - in Fig. 11, where binding sites on a different side of the peptide chain are filled with Hyp. It is interesting to note that even though these positions are equivalent from QLPD energy point of view, the interacting amino acids differ (as seen in Fig. 11). Such binding multiplicity could contribute to the explanation of scBH1 increased fluorescent spectral intensity (Fig. 7).

3.6. Interaction profiles of anti-apoptotic Bcl2 proteins with Hyp and other BH3 mimetics

In accord with our preliminary measurements of Hyp effects on other anti-apoptotic Bcl2 proteins (unpublished data) as well as for comparison of Hyp and the other BH3 mimetics binding profiles, we performed further docking calculations. The resulting QPLD docking scores are summarized in Table 3 and the lowest-energy docking poses of ABT263 and Hyp of the three anti-apoptotic Bcl2 proteins are shown in Fig. 12.

Table 3 compares ligand binding energies to Bcl2, Bcl_{XL} and Mcl1. The comparison between ligands, based on QPLD docking scores, indicates that Hyp binding to Bcl2 is weaker than the binding of ABT263 or other known Bcl2 inhibitors. On the other hand, the QPLD docking indicates that Hyp may bind to Bcl_{XL} better than ABT263 or gossypol, and further that Hyp may be the best binder to Mcl1. These “in silico” predictions indicate possibility that Hyp may be a BH3 mimetic molecule, however, this hypothesis needs to be tested in further studies. To our knowledge, there is no published information available regarding Hyp effect on Bcl_{XL} or Mcl1.

The QPLD calculated binding prediction does not fully agree with the known binding constants for BH3 mimetics, especially for Bcl_{XL} where significant preference of ABT263 is apparent (Table 4). On the other hand, the cytotoxicity of BH3 mimetics (EC_{50}) (Table 5) does not always correspond to their specificity and binding constants (Table 4), and their effects depend on the makeup of expressed anti- and pro-apoptotic members of Bcl2 proteins and off-target mechanisms, involving activation of alternative cell death modes and modulation of multiple signaling pathways. Therefore, there are still numerous questions regarding the pharmacological effects of BH3 mimetics that contribute to their cytotoxic activity [20].

Comparison of chemo-informatics data (calculated by the Schrodinger QikProp program [120]) with predicted LD_{50} values [121] and published EC_{50} data [25,26,32,37,119,122,123] is summarized in Table 5. It is evident that the ligands can be grouped into two groups according their MW values, conformational flexibility and QikProp predicted octanol/water distribution coefficient. Common feature of the ligands is the number of the rings that varies between 4–8. The molecular polar surface (MPS) of the ligands varies between 132–183. This relatively small MPS variation of around 30% could play a role in the fact that the ligands exhibit closed similarity in binding site occupancy, as illustrated by Fig. 12.

4. Conclusion

Our work revealed interaction between Hyp and anti-apoptotic Bcl2 protein and that can plausibly explain Hyp light-independent cytotoxicity and its effect on Bcl2 proteins distributions. To our knowledge, this finding is novel and interaction between Hyp and Bcl2 proteins were not described, yet. Our present and previous findings together with all other published results [19,43–47,78–80,96] indicate that Hyp may function in numerous cell signaling pathways including acting as a BH3 mimetic.

We have shown that Hyp binds into the Bcl2 hydrophobic groove comprised of BH3 and BH1 domains. Furthermore, our molecular docking findings revealed that Hyp may also interact with other anti-apoptotic members of Bcl2 family, Bcl_{XL} and Mcl1 comparable to panBcl2 BH3 mimetics such as gossypol and TW37. The hydrophobic interactions were predominant for all these cases. The QPLD docking indicated that Hyp may be the best binder to Mcl1 and may bind to Bcl_{XL} better than ABT263 or gossypol. While the modeling findings need to be confirmed by *in vitro* studies, they certainly substantiate further investigation of Hyp effects on anti-apoptotic Mcl1 and Bcl_{XL}. We believe that our *in vitro* and *in silico* data together with the on-line predicted Hyp LD_{50} values lay the foundation for the investigation of Hyp as a novel BH3 mimetic molecule and its potential to enhance other cancer treatments.

Acknowledgements

We would like to thank NanoTemper Technologies GmbH and their people for allowing us to use their facilities in Krakow, Poland, to conclude our MST measurements. We especially thank their application specialist Jakub Nowak, PhpH.D. for his help. Further, Mgr. Kurt Magsamen, PJ Safarik University in Kosice, Slovakia and Dr. Anna Kozarova, University of Windsor, Windsor, Canada are highly acknowledged for critical reading and comments on the manuscript. Present work was supported by the Slovak Grant Agency VEGA 1/0425/15, 1/0208/16 and 1-0421-18; and by the Slovak Research and Development Agency APVV-15-0485 and APVV-16-0158.

Appendix A. Supplementary data

Supplementary material related to this article can be found, in the online version, at doi:https://doi.org/10.1016/j.pdpdt.2019.08.016.

References

[1] A.M. Petros, E.T. Olejniczak, S.W. Fesik, Structural biology of the Bcl-2 family of proteins, Biochim. Biophys. Acta 1644 (2004) 83–94.
[2] M. Certo, V. Del Gaizo Moore, M. Nishino, G. Wei, S. Korsmeyer, S.A. Armstrong, et al., Mitochondria primed by death signals determine cellular addiction to antiapoptotic BCL-2 family members, Cancer Cell 9 (2006) 351–365.
[3] F. Llambi, T. Moldoveanu, S.W. Tait, L. Bouchier-Hayes, J. Temirov, L.L. McCormick, et al., A unified model of mammalian BCL-2 protein family interactions at the mitochondria, Mol. Cell 44 (2011) 517–531.
[4] C. Correia, S.H. Lee, X.W. Meng, N.D. Vincelette, K.L. Knorr, H. Ding, et al., Emerging understanding of Bcl-2 biology: implications for neoplastic progression and treatment, Biochim. Biophys. Acta 1853 (2015) 1658–1671.
[5] M. Vogler, Targeting BCL2-Proteins for the treatment of solid tumours, Adv. Med. 2014 (2014) 943648.
[6] J.N. Gong, T. Khong, D. Segal, Y. Yao, C.D. Riffkin, J.M. Garnier, et al., Hierarchy for targeting prosurvival BCL2 family proteins in multiple myeloma: pivotal role of MCL1, Blood 128 (2016) 1834–1844.
[7] Q. Huang, A.M. Petros, H.W. Virgin, S.W. Fesik, E.T. Olejniczak, Solution structure of a Bcl-2 homolog from Kaposi’s sarcoma virus, Proc Natl Acad Sci. 99 (2002) 3428–3433.
[8] Q. Huang, A.M. Petros, H.W. Virgin, S.W. Fesik, E.T. Olejniczak, Solution structure of the BHRF1 protein from Epstein-Barr virus, a homolog of human Bcl-2, J. Mol. Biol. 332 (2003) 1123–1130.
[9] J. DeBartolo, S. Dutta, L. Reich, A.E. Keating, Predictive Bcl-2 family binding models rooted in experiment or structure, J. Mol. Biol. 422 (2012) 124–144.
[10] A. Letai, M.C. Bassik, L.D. Walensky, M.D. Sorcinelli, S. Weiler, S.J. Korsmeyer, Distinct BH3 domains either sensitize or activate mitochondrial apoptosis, serving as prototype cancer therapeutics, Cancer Cell 2 (2002) 183–192.
[11] R.T. Uren, G. Dewson, L. Chen, S.C. Coyne, D.C. Huang, J.M. Adams, et al., Mitochondrial permeabilization relies on BH3 ligands engaging multiple prosurvival Bcl-2 relatives, not Bak, J. Cell Biol. 177 (2007) 277–287.
[12] M. Kvansakul, M.G. Hinds, Structural biology of the Bcl-2 family and its mimicry by viral proteins, Cell Death Dis. 4 (2013) e909.
[13] J.L. Wang, Z.J. Zhang, S. Choksi, S. Shan, Z. Lu, C.M. Croce, et al., Cell permeable Bcl-2 binding peptides: a chemical approach to apoptosis induction in tumor cells, Cancer Res. 60 (2000) 1498–1502.
[14] P.K. Raghav, Y.K. Verma, G.U. Gangenahalli, Peptide screening to knockdown Bcl-2′s anti-apoptotic activity: implications in cancer treatment, Int. J. Biol. Macromol. 50 (2012) 796–814.
[15] J.L. Wang, D.X. Liu, Z.J. Zhang, S.M. Shan, X.B. Han, S.M. Srinivasula, et al., Structure-based discovery of an organic compound that binds Bcl-2 protein and induces apoptosis of tumor cells, Proc Natl Acad Sci U S A. 97 (2000) 7124–7129.
[16] G. Wang, Z. Nikolovska-Coleska, C.Y. Yang, R. Wang, G. Tang, J. Guo, et al., Structure-based design of potent small-molecule inhibitors of anti-apoptotic Bcl-2 proteins, J. Med. Chem. 49 (2006) 6139–6142.
[17] J. O’Neill, M. Manion, P. Schwartz, D.M. Hockenbery, Promises and challenges of

targeting Bcl-2 anti-apoptotic proteins for cancer therapy, Biochim. Biophys. Acta 1705 (2004) 43–51.
[18] A.S. Azmi, R.M. Mohammad, Non-peptidic small molecule inhibitors against Bcl-2 for cancer therapy, J. Cell. Physiol. 218 (2009) 13–21.
[19] M.S. Davids, A. Letai, Targeting the B-cell lymphoma/leukemia 2 family in cancer, J. Clin. Oncol. 30 (2012) 3127–3135.
[20] L. Vela, I. Marzo, Bcl-2 family of proteins as drug targets for cancer chemotherapy: the long way of BH3 mimetics from bench to bedside, Curr. Opin. Pharmacol. 23 (2015) 74–81.
[21] M.P.A. Luna-Vargas, J.E. Chipuk, Physiological and pharmacological control of BAK, BAX, and beyond, Trends Cell Biol. 26 (2016) 906–917.
[22] T. Oltersdorf, S.W. Elmore, A.R. Shoemaker, R.C. Armstrong, D.J. Augeri, B.A. Belli, et al., An inhibitor of Bcl-2 family proteins induces regression of solid tumours, Nature 435 (2005) 677–681.
[23] M.F. Rega, M. Leone, D. Jung, N.J. Cotton, J.L. Stebbins, M. Pellecchia, Structure-based discovery of a new class of Bcl-xL antagonists, Bioorg. Chem. 35 (2007) 344–353.
[24] S. Trudel, Z.H. Li, J. Rauw, R.E. Tiedemann, X.Y. Wen, A.K. Stewart, Preclinical studies of the pan-Bcl inhibitor obatoclax (GX015-070) in multiple myeloma, Blood 109 (2007) 5430–5438.
[25] C. Tse, A.R. Shoemaker, J. Adickes, M.G. Anderson, J. Chen, S. Jin, et al., ABT-263: a potent and orally bioavailable Bcl-2 family inhibitor, Cancer Res. 68 (2008) 3421–3428.
[26] V. Voss, C. Senft, V. Lang, M.W. Ronellenfitsch, J.P. Steinbach, V. Seifert, et al., The pan-Bcl-2 inhibitor (-)-gossypol triggers autophagic cell death in malignant glioma, Mol. Cancer Res. 8 (2010) 1002–1016.
[27] J. Lian, X. Wu, F. He, D. Karnak, W. Tang, Y. Meng, et al., A natural BH3 mimetic induces autophagy in apoptosis-resistant prostate cancer via modulating Bcl-2–Beclin1 interaction at endoplasmic reticulum, Cell Death Differ. 18 (2011) 60–71.
[28] S.J. Chmura, M.E. Dolan, A. Cha, H.J. Mauceri, D.W. Kufe, R.R. Weichselbaum, In vitro and in vivo activity of protein kinase C inhibitor chelerythrine chloride induces tumor cell toxicity and growth delay in vivo, Clin. Cancer Res. 6 (2000) 737–742.
[29] S.P. Tzung, K.M. Kim, G. Basanez, C.D. Giedt, J. Simon, J. Zimmerberg, et al., Antimycin A mimics a cell-death-inducing Bcl-2 homology domain 3, Nat. Cell Biol. 3 (2001) 183–191.
[30] P. Miskovsky, Hypericin–a new antiviral and antitumor photosensitizer: mechanism of action and interaction with biological macromolecules, Curr. Drug Targets 3 (2002) 55–84.
[31] A. Karioti, A.R. Bilia, Hypericins as potential leads for new therapeutics, Int. J. Mol. Sci. 11 (2010) 562–594.
[32] B. Martinez-Poveda, A.R. Quesada, M.A. Medina, Hypericin in the dark inhibits key steps of angiogenesis in vitro, Eur. J. Pharmacol. 516 (2005) 97–103.
[33] E.B. Gyenge, D. Luscher, P. Forny, M. Antoniol, G. Geisberger, H. Walt, et al., Photodynamic mechanisms induced by a combination of hypericin and a chlorin based-photosensitizer in head and neck squamous cell carcinoma cells, Photochem. Photobiol. 89 (2013) 150–162.
[34] P. Larisch, T. Verwanger, K. Onder, B. Krammer, In vitro analysis of photosensitizer accumulation for assessment of applicability of fluorescence diagnosis of squamous cell carcinoma of epidermolysis bullosa patients, Biomed Res. Int. 2013 (2013) 521281.
[35] P. Larisch, T. Verwanger, M. Linecker, B. Krammer, The interrelation between a pro-inflammatory milieu and fluorescence diagnosis or photodynamic therapy of human skin cell lines, Photodiagnosis Photodyn. Ther. 11 (2014) 91–103.
[36] J. Berlanda, T. Kiesslich, V. Engelhardt, B. Krammer, K. Plaetzer, Comparative in vitro study on the characteristics of different photosensitizers employed in PDT, J. Photochem. Photobiol. B 100 (2010) 173–180.
[37] V. Huntosova, M. Novotova, Z. Nichtova, L. Balogova, M. Maslanakova, D. Petrovajova, et al., Assessing light-independent effects of hypericin on cell viability, ultrastructure and metabolism in human glioma and endothelial cells, Toxicol. In Vitro 40 (2017) 184–195.
[38] R. Rizzuto, P. Pinton, W. Carrington, F.S. Fay, K.E. Fogarty, L.M. Lifshitz, et al., Close contacts with the endoplasmic reticulum as determinants of mitochondrial Ca2+ responses, Science 280 (1998) 1763–1766.
[39] O.M. de Brito, L. Scorrano, An intimate liaison: spatial organization of the endoplasmic reticulum-mitochondria relationship, EMBO J. 29 (2010) 2715–2723.
[40] L. Balogova, M. Maslanakova, L. Dzurova, P. Miskovsky, K. Stroffekova, Bcl-2 proapoptotic proteins distribution in U-87 MG glioma cells before and after hypericin photodynamic action, Gen. Physiol. Biophys. 32 (2013) 179–187.
[41] M.G. Annis, N. Zamzami, W. Zhu, L.Z. Penn, G. Kroemer, B. Leber, et al., Endoplasmic reticulum localized Bcl-2 prevents apoptosis when redistribution of cytochrome c is a late event, Oncogene 20 (2001) 1939–1952.
[42] B. Gajkowska, T. Motyl, H. Olszewska-Badarczuk, M.M. Godlewski, Expression of BAX in cell nucleus after experimentally induced apoptosis revealed by immunogold and embedment-free electron microscopy, Cell Biol. Int. 25 (2001) 725–733.
[43] S.A. Mirmalek, M.A. Azizi, E. Jangholi, S. Yadollah-Damavandi, M.A. Javidi, Y. Parsa, et al., Cytotoxic and apoptogenic effect of hypericin, the bioactive component of Hypericum perforatum on the MCF-7 human breast cancer cell line, Cancer Cell Int. 16 (2015) 3.
[44] M. Acar, Z. Ocak, K. Erdogan, E.N. Cetin, O.F. Hatipoglu, U. Uyeturk, et al., The effects of hypericin on ADAMTS and p53 gene expression in MCF-7 breast cancer cells, JBUON 19 (2014) 627–632.
[45] M. Blank, G. Lavie, M. Mandel, S. Hazan, A. Orenstein, D. Meruelo, et al., Antimetastatic activity of the photodynamic agent hypericin in the dark, Int. J. Cancer 111 (2004) 596–603.
[46] M. Mandel, M. Blank, S. Hazan, Y. Keisari, G. Lavie, ANTI-cancer activities of hypericin in the dark¶, Photochem. Photobiol. 74 (2007) 120–125.
[47] M. Roelants, B. Van Cleynenbreugel, E. Lerut, H. Van Poppel, P.A. de Witte, Human serum albumin as key mediator of the differential accumulation of hypericin in normal urothelial cell spheroids versus urothelial cell carcinoma spheroids, Photochem. Photobiol. Sci. 10 (2011) 151–159.
[48] A.B. Uzdensky, D.E. Bragin, M.S. Kolosov, A. Kubin, H.G. Loew, J. Moan, Photodynamic effect of hypericin and a water-soluble derivative on isolated crayfish neuron and surrounding glial cells, J. Photochem. Photobiol. B, Biol. 72 (2003) 27–33.
[49] S. Noell, D. Mayer, W.S. Strauss, M.S. Tatagiba, R. Ritz, Selective enrichment of hypericin in malignant glioma: pioneering in vivo results, Int. J. Oncol. 38 (2011) 1343–1348.
[50] Z. Diwu, Novel therapeutic and diagnostic applications of hypocrellins and hypericins, Photochem. Photobiol. 61 (1995) 529–539.
[51] P. Agostinis, A. Vandenbogaerde, A. Donella-Deana, L.A. Pinna, K.T. Lee, J. Goris, et al., Photosensitized inhibition of growth factor-regulated protein kinases by hypericin, Biochem. Pharmacol. 49 (1995) 1615–1622.
[52] P. Agostinis, A. Donella-Deana, J. Cuveele, A. Vandenbogaerde, S. Sarno, W. Merlevede, et al., A comparative analysis of the photosensitized inhibition of growth-factor regulated protein kinases by hypericin-derivatives, Biochem. Biophys. Res. Commun. 220 (1996) 613–617.
[53] M. Halder, P.K. Chowdhury, R. Das, P. Mukherjee, W.M. Atkins, J.W. Petrich, Interaction of glutathione S-transferase with hypericin: a photophysical study, J. Phys. Chem. B 109 (2005) 19484–19489.
[54] K. Das, A.V. Smirnov, J. Wen, P. Miskovsky, J.W. Petrich, Photophysics of hypericin and hypocrellin A in complex with subcellular components: interactions with human serum albumin, Photochem. Photobiol. 69 (1999) 633–645.
[55] P. Miskovsky, J. Hritz, S. Sanchez-Cortes, G. Fabriciova, J. Ulicny, L. Chinsky, Interaction of hypericin with serum albumins: surface-enhanced Raman spectroscopy, resonance Raman spectroscopy and molecular modeling study, Photochem. Photobiol. 74 (2001) 172–183.
[56] P. Mukherjee, R. Adhikary, M. Halder, J.W. Petrich, P. Miskovsky, Accumulation and interaction of hypericin in low-density lipoprotein–a photophysical study, Photochem. Photobiol. 84 (2008) 706–712.
[57] H.R. Vardapetyan, A.S. Martirosyan, S.G. Tiratsuyan, A.A. Hovhannisyan, Interaction between hypericin and hemoglobin, J. Photochem. Photobiol. B 101 (2010) 53–58.
[58] T. Youssef, Fluorescence study on the interaction between hypericin and lens protein "alpha-crystallin, Photochem. Photobiol. 85 (2009) 921–926.
[59] M. Huls, M. Ott, M.G. Cornelius, G. Fricker, St. John's Wort Constituents Modulate P-glycoprotein Transport Activity at the Blood-Brain Barrier, Pharm. Res. 27 (2010) 811–822.
[60] V. Verebova, D. Belej, J. Joniova, Z. Jurasekova, P. Miskovsky, T. Kozar, et al., Deeper insights into the drug defense of glioma cells against hydrophobic molecules, Int. J. Pharm. 503 (2016) 56–67.
[61] S. Kocanova, T. Hornakova, J. Hritz, D. Jancura, D. Chorvat, A. Mateasik, et al., Characterization of the interaction of hypericin with protein kinase C in U-87 MG human glioma cells, Photochem. Photobiol. 82 (2006) 720.
[62] Maestro, Version 10.3.015. Schrödinger Release 2015-3, Schrödinger, LLC, New York, NY, 2015.
[63] B.B. Toure, K. Miller-Moslin, N. Yusuff, L. Perez, M. Dore, C. Joud, et al., The role of the acidity of N-heteroaryl sulfonamides as inhibitors of bcl-2 family protein-protein interactions, ACS Med. Chem. Lett. 4 (2013) 186–190.
[64] T. Halgren, New method for fast and accurate binding-site identification and analysis, Chem. Biol. Drug Des. 69 (2007) 146–148.
[65] T.A. Halgren, Identifying and characterizing binding sites and assessing druggability, J. Chem. Inf. Model. 49 (2009) 377–389.
[66] A.D. Bochevarov, E. Harder, T.F. Hughes, J.R. Greenwood, D.A. Braden, D.M. Philipp, et al., Jaguar: a high-performance quantum chemistry software program with strengths in life and materials sciences, Int. J. Quantum Chem. 113 (2013) 2110–2142.
[67] A.E. Cho, V. Guallar, B.J. Berne, R. Friesner, Importance of accurate charges in molecular docking: quantum mechanical/molecular mechanical (QM/MM) approach, J. Comput. Chem. 26 (2005) 915–931.
[68] O. Trott, A.J. Olson, AutoDock Vina: improving the speed and accuracy of docking with a new scoring function, efficient optimization, and multithreading, J. Comput. Chem. 31 (2010) 455–461.
[69] S. Salentin, S. Schreiber, V.J. Haupt, M.F. Adasme, M. Schroeder, PLIP: fully automated protein-ligand interaction profiler, Nucleic Acids Res. 43 (2015) W443–7.
[70] S.A. Seidel, P.M. Dijkman, W.A. Lea, G. van den Bogaart, M. Jerabek-Willemsen, A. Lazic, et al., Microscale thermophoresis quantifies biomolecular interactions under previously challenging conditions, Methods 59 (2013) 301–315.
[71] M. Jerabek-Willemsen, T. Andre, R. Wanner, H.M. Roth, S. Duhr, P. Baaske, et al., MicroScale thermophoresis: interaction analysis and beyond, J. Mol. Struct. 1077 (2014) 101–113.
[72] P. Baaske, C.J. Wienken, P. Reineck, S. Duhr, D. Braun, Optical thermophoresis for quantifying the buffer dependence of aptamer binding, Angew. Chem. Int. Ed. Engl. 49 (2010) 2238–2241.
[73] L. Rieger, M. Weller, A. Bornemann, M. Schabet, J. Dichgans, R. Meyermann, BCL-2 family protein expression in human malignant glioma: a clinical-pathological correlative study, J. Neurol. Sci. 155 (1998) 68–75.
[74] F. Wang, K. Bhat, M. Doucette, S. Zhou, Y. Gu, B. Law, et al., Docosahexaenoic acid (DHA) sensitizes brain tumor cells to etoposide-induced apoptosis, Curr. Mol. Med. 11 (2011) 503–511.

[75] J. Lindsay, M.D. Esposti, A.P. Gilmore, Bcl-2 proteins and mitochondria—specificity in membrane targeting for death, Biochimica et Biophysica Acta (BBA)-Molecular Cell Research. 1813 (2011) 532–539.
[76] M. Maslanakova, L. Balogova, P. Miskovsky, R. Tkacova, K. Stroffekova, Anti- and Pro-apoptotic Bcl2 Proteins Distribution and Metabolic Profile in Human Coronary Aorta Endothelial Cells Before and After HypPDT, Cell Biochem. Biophys. 74 (2016) 435–447.
[77] M. Misuth, J. Joniova, D. Horvath, L. Dzurova, Z. Nichtova, M. Novotova, et al., The flashlights on a distinct role of protein kinase C delta: phosphorylation of regulatory and catalytic domain upon oxidative stress in glioma cells, Cell. Signal. 34 (2017) 11–22.
[78] L.H. Huang, J.Q. Hu, W.Q. Tao, Y.H. Li, G.M. Li, P.Y. Xie, et al., Gossypol inhibits phosphorylation of Bcl-2 in human leukemia HL-60 cells, Eur. J. Pharmacol. 645 (2010) 9–13.
[79] Z. Zhang, T. Song, T. Zhang, J. Gao, G. Wu, L. An, et al., A novel BH3 mimetic S1 potently induces Bax/Bak-dependent apoptosis by targeting both Bcl-2 and Mcl-1, Int. J. Cancer 128 (2010) 1724–1735.
[80] V. Fresquet, M. Rieger, C. Carolis, M.J. Garcia-Barchino, J.A. Martinez-Climent, Acquired mutations in BCL2 family proteins conferring resistance to the BH3 mimetic ABT-199 in lymphoma, Blood 123 (2014) 4111–4119.
[81] L. Dzurova, D. Petrovajova, Z. Nadova, V. Huntosova, P. Miskovsky, K. Stroffekova, The role of anti-apoptotic protein kinase Cα in response to hypericin photodynamic therapy in U-87 MG cells, Photodiagnosis Photodyn. Ther. 11 (2014) 213–226.
[82] Q.L. Lu, A.M. Hanby, M.A.N. Hajibagheri, S.E. Gschmeissner, P.J. Lu, J. Taylorpapadimitriou, et al., Bcl-2 protein localizes to the chromosomes of mitotic nuclei and is correlated with the cell-cycle in cultured epithelial-cell lines, J. Cell. Sci. 107 (1994) 363–371.
[83] R. Hoetelmans, H.J. van Slooten, R. Keijzer, S. Erkeland, C.J. van de Velde, J.H. Dierendonck, Bcl-2 and Bax proteins are present in interphase nuclei of mammalian cells, Cell Death Differ. 7 (2000) 384–392.
[84] X. Deng, F. Gao, W.S. May Jr., Bcl2 retards G1/S cell cycle transition by regulating intracellular ROS, Blood 102 (2003) 3179–3185.
[85] B.P. Portier, G. Taglialatela, Bcl-2 localized at the nuclear compartment induces apoptosis after transient overexpression, J. Biol. Chem. 281 (2006) 40493–40502.
[86] Q. Wang, F. Gao, W.S. May, Y. Zhang, T. Flagg, X. Deng, Bcl2 negatively regulates DNA double-strand-break repair through a nonhomologous end-joining pathway, Mol. Cell 29 (2008) 488–498.
[87] C. Bokemeyer, C. Oing, P. Tennstedt, R. Simon, J. Volquardsen, K. Borgmann, et al., BCL2-overexpressing prostate cancer cells rely on PARP1-dependent end-joining and are sensitive to combined PARP inhibitor and radiation therapy, Cancer Lett. 423 (2018) 60–70.
[88] T.S. Kumar, V. Kari, B. Choudhary, M. Nambiar, T.S. Akila, S.C. Raghavan, Anti-apoptotic protein BCL2 down-regulates DNA end joining in cancer cells, J. Biol. Chem. 285 (2010) 32657–32670.
[89] B.-H. Choi, G. Chakraborty, K. Baek, H.S. Yoon, Aspirin-induced Bcl-2 translocation and its phosphorylation in the nucleus trigger apoptosis in breast cancer cells, Exp. Mol. Med. 45 (2013) e47–e.
[90] J. Liu, W. Zhou, S.S. Li, Z. Sun, B. Lin, Y.Y. Lang, et al., Modulation of orphan nuclear receptor Nur77-mediated apoptotic pathway by acetylshikonin and analogues, Cancer Res. 68 (2008) 8871–8880.
[91] P.P. Ruvolo, X. Deng, B.K. Carr, W.S. May, A functional role for mitochondrial protein kinase Calpha in Bcl2 phosphorylation and suppression of apoptosis, J. Biol. Chem. 273 (1998) 25436–25442.
[92] X. Deng, F. Gao, T. Flagg, W.S. May Jr., Mono- and multisite phosphorylation enhances Bcl2′s antiapoptotic function and inhibition of cell cycle entry functions, Proc Natl Acad Sci U S A. 101 (2004) 153–158.
[93] X. Deng, S.M. Kornblau, P.P. Ruvolo, W.S. May, Regulation of Bcl2 phosphorylation and potential significance for leukemic cell chemoresistance, JNCI Monographs. 2000 (2000) 30–37.
[94] S. Kascakova, Z. Nadova, A. Mateasik, J. Mikes, V. Huntosova, M. Refregiers, et al., High level of low-density lipoprotein receptors enhance hypericin uptake by U-87 MG cells in the presence of LDL, Photochem. Photobiol. 84 (2008) 120–127.
[95] V. Huntosova, Z. Nadova, L. Dzurova, V. Jakusova, F. Sureau, P. Miskovsky, Cell death response of U87 glioma cells on hypericin photoactivation is mediated by dynamics of hypericin subcellular distribution and its aggregation in cellular organelles, Photochem. Photobiol. Sci. 11 (2012) 1428–1436.
[96] P. Gao, C. Bauvy, S. Souquere, G. Tonelli, L. Liu, Y. Zhu, et al., The Bcl-2 homology domain 3 mimetic gossypol induces both Beclin 1-dependent and Beclin 1-independent cytoprotective autophagy in cancer cells, J. Biol. Chem. 285 (2010) 25570–25581.
[97] M. Opydo-Chanek, O. Gonzalo, I. Marzo, Multifaceted anticancer activity of BH3 mimetics: current evidence and future prospects, Biochem. Pharmacol. 136 (2017) 12–23.
[98] C. Zhao, S. Yin, Y. Dong, X. Guo, L. Fan, M. Ye, et al., Autophagy-dependent EIF2AK3 activation compromises ursolic acid-induced apoptosis through upregulation of MCL1 in MCF-7 human breast cancer cells, Autophagy 9 (2013) 196–207.
[99] B. Wang, Z. Ni, X. Dai, L. Qin, X. Li, L. Xu, et al., The Bcl-2/xL inhibitor ABT-263 increases the stability of Mcl-1 mRNA and protein in hepatocellular carcinoma cells, Mol. Cancer 13 (2014) 98.
[100] Y.C. Lee, L.J. Wang, C.H. Huang, Y.J. Shi, L.S. Chang, ABT-263-induced MCL1 upregulation depends on autophagy-mediated 4EBP1 downregulation in human leukemia cells, Cancer Lett. 432 (2018) 191–204.
[101] M.C. Maiuri, A. Criollo, E. Tasdemir, J.M. Vicencio, N. Tajeddine, J.A. Hickman, et al., BH3-only proteins and BH3 mimetics induce autophagy by competitively disrupting the interaction between beclin 1 and Bcl-2/Bcl-XL, Autophagy 3 (2014) 374–376.
[102] P.V. Troshin, J.B. Procter, G.J. Barton, Java bioinformatics analysis web services for multiple sequence alignment–JABAWS:MSA, Bioinformatics 27 (2011) 2001–2002.
[103] R.W. Alston, M. Lasagna, G.R. Grimsley, J.M. Scholtz, G.D. Reinhart, C.N. Pace, Peptide sequence and conformation strongly influence tryptophan fluorescence, Biophys. J. 94 (2008) 2280–2287.
[104] P.L. Muino, P.R. Callis, Solvent effects on the fluorescence quenching of tryptophan by amides via electron transfer. Experimental and computational studies, J. Phys. Chem. B 113 (2009) 2572–2577.
[105] B.N. Markiewicz, D. Mukherjee, T. Troxler, F. Gai, Utility of 5-Cyanotryptophan fluorescence as a sensitive probe of protein hydration, J. Phys. Chem. B 120 (2016) 936–944.
[106] J.A. Encinar, J.A. Poveda, M. Prieto, J.M. Gonzalez-Ros, C.R. Mateo, Intrinsic tyrosine fluorescence as a tool to study the interaction of the shaker B “ball” peptide with anionic membranes, Biochemistry 42 (2003) 7124–7132.
[107] J.R. Lakowicz, Principles of Fluorescence Spectroscopy, 3rd ed., Springer, New York, 2006.
[108] K.B. Davis, Z. Zhang, E.A. Karpova, J. Zhang, Application of tyrosine-tryptophan fluorescence resonance energy transfer in monitoring protein size changes, Anal. Biochem. 557 (2018) 142–150.
[109] H. Huang, A.L. McIntosh, G.G. Martin, K.K. Landrock, D. Landrock, S. Gupta, et al., Structural and functional interaction of fatty acids with human liver fatty acid-binding protein (L-FABP) T94A variant, FEBS J. 281 (2014) 2266–2283.
[110] W.H. Qiu, T.P. Li, L.Y. Zhang, Y. Yang, Y.T. Kao, L.J. Wang, et al., Ultrafast quenching of tryptophan fluorescence in proteins: interresidue and intrahelical electron transfer, Chem. Phys. 350 (2008) 154–164.
[111] J.P. Douliez, T. Michon, D. Marion, Steady-state tyrosine fluorescence to study the lipid-binding properties of a wheat non-specific lipid-transfer protein (nsLTP1), Biochimica Et Biophysica Acta-Biomembranes. 1467 (2000) 65–72.
[112] H.T. Hsu, Y.H. Tseng, Y.L. Chou, S.H. Su, Y.H. Hsu, B.Y. Chang, Characterization of the RNA-binding properties of the triple-gene-block protein 2 of Bamboo mosaic virus, Virol. J. 6 (2009) 50.
[113] R.W. Birkinshaw, P.E. Czabotar, The BCL-2 family of proteins and mitochondrial outer membrane permeabilisation, Semin. Cell Dev. Biol. 72 (2017) 152–162.
[114] J.G. Varnes, T. Gero, S. Huang, R.B. Diebold, C. Ogoe, P.T. Grover, et al., Towards the next generation of dual Bcl-2/Bcl-xL inhibitors, Bioorg. Med. Chem. Lett. 24 (2014) 3026–3033.
[115] D. Freeman, F. Frolow, E. Kapinus, D. Lavie, G. Lavie, D. Meruelo, et al., Acidic properties of hypericin and its octahydroxy analogue in the ground and excited states, J. Chem. Soc. Chem. Commun. 891 (1994).
[116] H. Falk, From the photosensitizer hypericin to the photoreceptor stentorin— the chemistry of phenanthroperylene quinones, Angew. Chemie Int. Ed. 38 (1999) 3116–3136.
[117] G. Bano, J. Stanicova, D. Jancura, J. Marek, M. Bano, J. Ulicny, et al., On the diffusion of hypericin in dimethylsulfoxide/water mixtures-the effect of aggregation, J. Phys. Chem. B 115 (2011) 2417–2423.
[118] Y. Wan, N. Dai, Z. Tang, H. Fang, Small-molecule Mcl-1 inhibitors: emerging anti-tumor agents, Eur. J. Med. Chem. 146 (2018) 471–482.
[119] B.D. Zeitlin, E. Joo, Z. Dong, K. Warner, G. Wang, Z. Nikolovska-Coleska, et al., Antiangiogenic effect of TW37, a small-molecule inhibitor of Bcl-2, Cancer Res. 66 (2006) 8698–8706.
[120] Schrödinger Release 2015-3, Schrödinger, LLC, QikProp. New York, NY, 2015.
[121] P. Banerjee, A.O. Eckert, A.K. Schrey, R. Preissner, ProTox-II: a webserver for the prediction of toxicity of chemicals, Nucleic Acids Res. 46 (2018) W257–W263.
[122] A.R. Shoemaker, M.J. Mitten, J. Adickes, S. Ackler, M. Refici, D. Ferguson, et al., Activity of the Bcl-2 family inhibitor ABT-263 in a panel of small cell lung cancer xenograft models, Clin. Cancer Res. 14 (2008) 3268–3277.
[123] R.M. Mohammad, A.S. Goustin, A. Aboukameel, B. Chen, S. Banerjee, G. Wang, et al., Preclinical studies of TW-37, a new nonpeptidic small-molecule inhibitor of Bcl-2, in diffuse large cell lymphoma xenograft model reveal drug action on both Bcl-2 and Mcl-1, Clin. Cancer Res. 13 (2007) 2226–2235.